Unusual, hierarchically structured composite of sugarcane pulp bagasse biochar loaded with Cu/Ni bimetallic nanoparticles for dye removal

Mengqi Tang, Youssef Snoussi, Arvind Bhakta, Mohamed El Garah, Ahmed Khalil, Souad Ammar, Mohamed Chehimi

Unusual, hierarchically structured composite of sugarcane pulp bagasse biochar loaded with Cu/Ni bimetallic nanoparticles for dye removal

Mengqi Tang[1], Youssef Snoussi[1#], Arvind K. Bhakta[1#], Mohamed El Garah[2,3#], Ahmed M. Khalil[4], Souad Ammar[1], Mohamed M. Chehimi[1,*]

1 Université Paris Cité, CNRS, ITODYS (UMR 7086), Paris 75013, France
2 LASMIS, Antenne de Nogent – 52, Pôle Technologique de Sud – Champagne, 52800 Nogent, France
3 Nogent International Center for CVD Innovation (NICCI), LRC CEA-LASMIS, Pôle Technologique de Sud Champagne, 52800 Nogent, France
4 Photochemistry Department, National Research Centre, Dokki, Giza 12622, Egypt

***Corresponding authors:** Mohamed M. Chehimi & Mengqi Tang, Université Paris Cité & CNRS, mohamed.chehimi@cnrs.fr ; mengqi.tang@etu.u-paris.fr

[#]These authors have contributed to this work equally.

Graphical Abstract

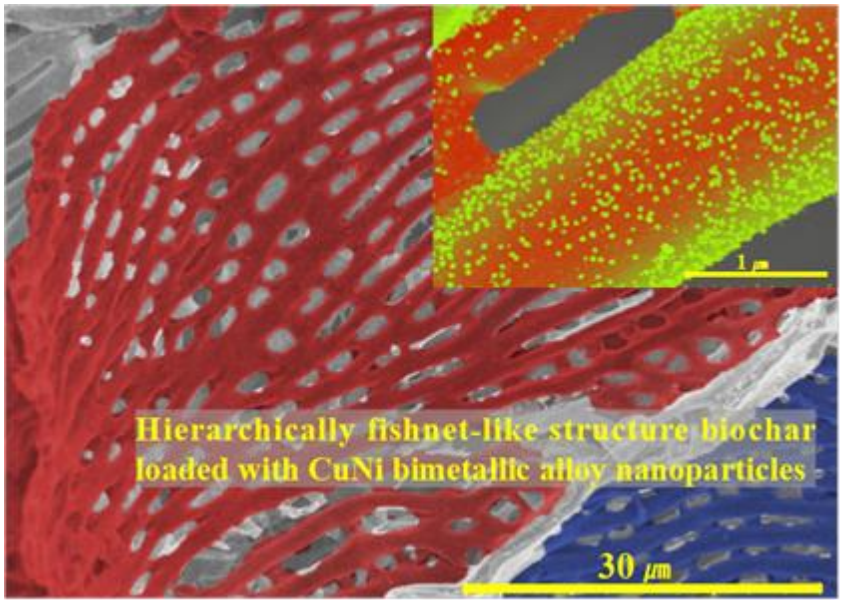

Abstract

Biochar-supported nanocatalysts emerged as unique materials for environmental remediation. Herein, sugarcane pulp bagasse (SCPB) was wet-impregnated with $Cu(NO_3)_2 3H_2O$ and $Ni(NO_3)_2 6H_2O$, then pyrolyzed at 500 °C, under N_2, for 1 hour. We specifically focused on sugarcane pulp instead of SCB and biochar materials. The metal nitrate to biomass ratio was set at 0.5, 1, and 2 mmol/g, with Cu/Ni initial ratio = 1. The process provided hierarchically structured porous biochar, topped with evenly dispersed 40 nm-sized CuNi alloy nanoparticles (SCPBB@CuNi). The biochar exhibited an unusual fishing net-like structure induced by nickel, with slits having a length in the 3-12 μm range. Such a fishing net-like porous structure was obtained without any harsh acidic or basic treatment of the biomass. It was induced, during pyrolysis, by the nanocatalysts or their precursors. The CuNi nanoparticles form true alloy as proved by XRD, and are prone to agglomeration at high initial metal nitrate concentration (2 mmol/g). Stepwise metal loading was probed by XPS versus the initial metal nitrate concentration. This is also reflected in the thermal gravimetric analyses. The SCPBB@CuNi / H_2O_2 (catalyst dose: 0.25 g/L) system served for the catalyzed removal of Malachite Green (MG), Methylene Blue (MB), and Methyl Orange (MO) dyes (concentration= 0.01 mmol/L). Both single and mixed dye solutions were treated in this advanced oxidation process (AOP). The dyes were removed in less than 30 min for MG and 3 h for MB, respectively, but 8 h for MO, therefore showing selectivity for the degradation of MG, under optimized degradation conditions. The catalysts could be collected with a magnet and reused three times, without any significant loss of activity (~ 85 %). AOP conditions did not induce any nanocatalyst leaching.

To sum up, we provide a simple wet impregnation route that permitted to design highly active Fenton-like biochar@CuNi composite catalyst for the degradation of organic pollutants, under daylight conditions.

Keywords:

Saccharum officinarum; biochar; bimetallic nanoalloy; porous materials; Fenton-like reaction; water treatment.

1. Introduction

The world is witnessing unprecedented technological and industrial expansion, causing real environmental and climate issues that are terrifyingly impacting Human health and well-being (Liu, Jiang et al. 2015). Meanwhile, many efforts are constantly devoted to implementing eco-friendly, cost-effective, and sustainable policies in order to face problems threatening planet Earth, especially those related to water (Ali, Burakova et al. 2019, Ali, Kon'kova et al. 2021) and air contamination (Hamouma, Kaur et al. 2019, Huang, Su et al. 2019) organic molecules and gases. Indeed, political decisions worldwide aim to maintain the balance between ecosystem preservation, economy, and social benefits (Low and Yee 2021). Convention on Climate Change (COP) is one of the most important events where politicians and environmental experts meet to change rules for a safer environment.

Taking the sole example of agro-wastes from the agro-industry and the agricultural activities, their management, recycling, and valorization is a highly challenging field. Indeed, billions of tons are yearly produced and must be managed, *e.g.* the World production of raw sugarcane was estimated to be 1.9 billion tons which once processed generate around 513 million metric tons of lignocellulosic waste (Pan, Zabed et al. 2022).

Besides animal feeding and fertilization, several innovative solutions have been proposed and employed to convert agro-wastes into green energy with low carbon dioxide emissions, *e.g.* bioethanol, biofuel or hydrogen (Adewuyi 2020, Ramlingam, Subramanian et al. 2022, Saravanan, Kumar et al. 2022), and also into functional bio-sourced material, for example, biochar (Tripathi, Sahu et al. 2016, Gopinath, Divyapriya et al. 2021, Aoulad El Hadj Ali, Ahrouch et al. 2022).

Biochar is a green and carbon-rich material made from the pyrolysis of diverse biomass wastes, at relatively moderate (400-600 °C) to high temperatures (above 700 °C), under oxygen-free (or low oxygen) conditions. It has emerged as a unique, low-cost material for agriculture, water treatment, and life sciences, to name but these

important domains. Biochar is coined “new black gold” (Nagula and Ramanjaneyulu 2020), for its exceptional physicochemical properties that can be tuned, and enhanced through modification (Goswami, Kushwaha et al. 2022). Such a modification of biochar is beneficial for pollutant adsorption (Ali, Afshinb et al. 2020), or for anchoring nanocatalysts onto the porous material for the complete mineralization of organic pollutants (Lopes and Astruc 2021, Yameen, AlMohamadi et al. 2023). Biochar with immobilized nanocatalysts constitute an emerging class of remarkably efficient advanced materials in water treatment (Shi, Deng et al. 2022), among other composites (Dihingia and Tiwari 2022) based on metal-organic frameworks (MOFs) (Xiao, Cheng et al. 2023), zeolites (Wang, Sun et al. 2021), mesoporous silica (Snoussi, Bastide et al. 2018, Verma, Kuwahara et al. 2020), carbon nitride (Tang, Cheng et al. 2023), to name but a few. However, biochar platforms are made from valueless biomass, therefore complying with the concept of *waste-to-wealth*, or *trash-to-treasure*.

There is a plethora of biomasses that are thermochemically converted into biochar, for example, agrowastes and side-products of the food and beverage industry. Particularly, sugarcane is the main product in the sugar industry; it grows rapidly and has a high yield worldwide (Aruna, Bagotia et al. 2021). A large amount of sugarcane bagasse as a by-product is discarded after processing. It follows that the conversion of SCB into biochar is an appealing strategy to elaborate highly performant catalysts and adsorbents for water treatment (Lopes and Astruc 2021, Sutar, Patil et al. 2022) and energy production (Kant Bhatia, Palai et al. 2021).

Of relevance to this contribution, the literature shows that bimetallic catalysts combine high activity and high selectivity metals (Pang, Wang et al. 2012). The addition of a second metallic component may affect the morphology and the electronic configuration of the final catalyst. The electronic effect, called also the ligand effect, results in more binding and active sites, hence a higher catalytic activity (Liao, Lo et al. 2015, Quiton, Lu et al. 2021, Chen, Liu et al. 2022) .

The incipient wet impregnation is most probably the simplest route to incorporate bimetallic catalysts into/onto the support matrix. The dispersing network is either co-impregnated with the bimetallic solution or successively impregnated with monometallic solutions (Quiton, Lu et al. 2021). Wet impregnation has always been considered a facile, cost-effective, and very efficient method to elaborate composite catalysts (Deraz 2018, Goswami, Kushwaha et al. 2022).

In our previous work, we synthesized several bimetallic biochar@catalyst materials with different structures by direct pyrolysis method and found that bimetallic nanoparticle/biochar are more active than the corresponding pure biochar and monometallic nanocomposites (Khalil, Michely et al. 2021, Omiri, Snoussi et al. 2022, Snoussi, Sifaoui et al. 2023). Transition metal nickel (Ni) is attractive due to its excellent magnetic properties and high activation ability of C-H and C-C bonds (Liao, Wang et al. 2018) but can suffer aggregation and consequently decreased catalytic efficiency (Gong, Ma et al. 2021). Copper is a less active transition metal but exhibits high selectivity (Hu, Yue et al. 2014). It is worth noting that the catalytic activity of CuNi is superior to those of the individual monometallic nanocatalysts, and bimetallic nanocatalysts dispersed on the support can avoid agglomeration and oxidation, hence the improved catalytic activity (Deka, Borah et al. 2019, Gong, Ma et al. 2021). Recently, we found that the copper-nickel/biochar served for the degradation of Methyl Orange and nickel imparted magnetic properties to the biochar (Khalil, Michely et al. 2021, Omiri, Snoussi et al. 2022). In another application, the group of Hassan Sheibani successfully synthesized CuNi bimetallic nanoparticles and mixed them with preformed pomegranate shell biochar to obtain a composite with excellent catalytic activity for the A3-coupling reactions (Zarei, Saidi et al. 2022). One key point is that copper precursors are low-cost, which makes CuNi bimetallic nanocatalyst of interest: cost-effective, catalytically highly active, magnetic, and thus easy to recover.

Despite the rich literature on CuNi bimetallic nanocatalysts, loading CuNi bimetallic nanocatalysts in- and on the surface of biochar remains sparse (Zhu, Wang

et al. 2019). Our ongoing research work consisted of the direct slow pyrolysis of biomass impregnated by copper and nickel nitrate mixtures under various conditions (Khalil, Michely et al. 2021, Omiri, Snoussi et al. 2022), instead of the in situ deposition of CuNi alloy onto pre-fabricated biochar (Zhu, Wang et al. 2019). Post-modification of biochar by nanocatalysts requires a chemical reductive process to convert the metal salts into metallic nanocatalysts, whereas mixing of biochar and CuNi bimetallic catalysts resulted in large immobilized particles (Zarei, Saidi et al. 2022), contrary to the wet impregnation approach before pyrolysis.

Returning to sugarcane, most of the research works on its thermochemical conversion to obtain biochar concerned the total sugarcane bagasse derived from sugarcane juice making. Instead, we were interested in removing the pulp from the total sugarcane bagasse to check if there is any interest in terms of physicochemical properties. Surprisingly, our first results indicated that sugarcane pulp bagasse loaded with copper and nickel nitrates led to unusual porous structure of the biochar with even distribution of narrow dispersion bimetallic CuNi nanoparticles (Tang, Snoussi et al. 2022). This has motivated us to conduct a comprehensive study on the preparation of new biochar@CuNi materials.

In this work, we report a simple and green method to prepare porous SCPBB@CuNi nanocomposites by slow pyrolysis, under nitrogen, of sugarcane pulp bagasse mixed with copper and nickel nitrates, through wet impregnation technique. The materials were characterized by X-ray diffraction (XRD), X-Ray photoelectron spectroscopy (XPS), Raman spectroscopy, scanning electron microscopy (SEM), and thermogravimetric analysis (TGA). The initial metal ion/sugarcane pulp has been monitored and the ratio set to 0.5, 1, and 2 mmol/g. This is an important parameter for controlling the extent of copper/nickel, the size, and the distribution of the nanoparticles on the biochar support. Moreover, biochar loaded with single metallic systems (biochar@Cu and biochar@Ni) served as control composites in order to understand the effect of each metal on the biochar structure. The biochar samples loaded with CuNi bimetallic nanoparticles were tested as catalysts of the degradation

of model dyes, namely Malachite Green (MG), Methyl Orange (MO), and Methylene Blue (MB), in the presence of H_2O_2 (advanced oxidation process, AOP). We have also tested the performances of the catalytic composites in the degradation of binary dye mixtures in order to investigate any competitive effects.

To the very best of our knowledge, this is the first report on biochar-supported CuNi bimetallic catalyst obtained by wet impregnation of sugarcane pulp bagasse and its slow pyrolysis for environmental remediation, *i.e.* dye degradation in water treatment applications.

2. Materials and methods

2.1. Biomass and Chemicals

The used sugarcane bagasse was cultivated and provided from Egypt (*Saccharum officinarum*). Sugarcane pulp bagasse (SCPB) agricultural was finely ground before use. Metal nitrate salts $Cu(NO_3)_2 \cdot 3H_2O$ and $Ni(NO_3)_2 \cdot 6H_2O$ were purchased from Aldrich and used as received. We used distilled water to dissolve metal nitrates before pyrolysis.

2.2. Synthesis of biochar loaded with Cu/Ni bimetallic nanoparticles

SCPB particles were impregnated with an aqueous solution of copper and nickel nitrates in the molar mass ratio of 0.5:0.5, 1:1, and 2:2, respectively (see Figure 1). The powder was mixed on a glass lens and dried at 60 degrees, overnight, until the powder weight was constant. Subsequently, the mixture containing metal salt-impregnated particles was transferred into a tubular furnace and pyrolyzed at 500 °C, under N_2 atmosphere for 1 h, with a heating rate of 20 °C min^{-1}. Copper and nickel nitrates were mixed in the deionized (DI) water. The final bimetallic nanoparticle-coated biochar samples are labeled SCPBB@CuNi-0.5, SCPBB@CuNi-1, and SCPBB@CuNi-2, respectively. The same agrowaste SCPB, without any metallic

nitrates, was pyrolyzed in the same conditions. We have also prepared SCPBB@Cu-0.5 and SCPBB@Ni-0.5 as reference materials.

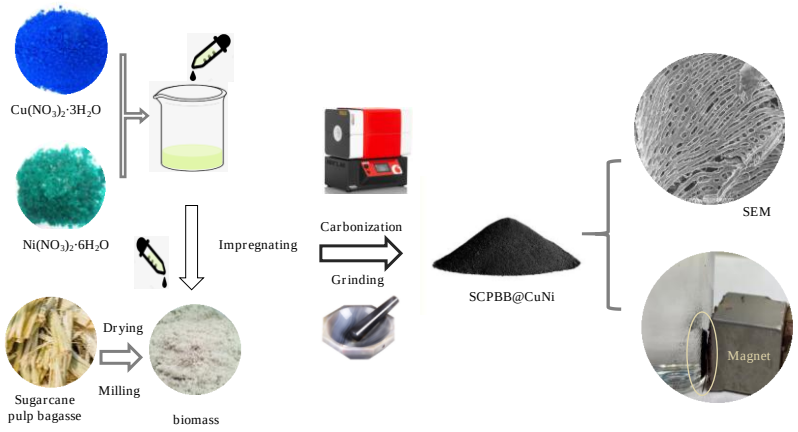

Figure 1. Schematic illustration for the copper nickel nanoparticle-loaded biochar SCPBB@CuNi by slow pyrolysis.

Table 1. Conditions for the preparation of pure and metallic nanoparticle-coated biochar by slow pyrolysis.

Materials	P-SCB Mass(g)	$Cu(NO_3)_2$•$3H_2O$ Mass (g)/mmol	$Ni(NO_3)_2$•$6H_2O$ Mass (g)/mmol	Distilled water (mL)	Before Pyrolyzed SCB+Metal Ion Mixture(g)	Biochar Mass (g) /Yield (%)	Experimental condition
SCPBB@CuNi-0.5	0.996	120.8/0.5	145.4/0.5	20	1.226	0.352/28.71	Temperature：500 °C Heating rate：20 °C · min Residence time：1 h Gas：N_2 atmosphere N_2 flow rate：2L· min^{-1}
SCPBB@CuNi-1	0.998	241.6/1	290.8/1	20	1.3195	0.441/33.41	
SCPBB@CuNi-2	0.997	483.2/2	581.6/2	20	1.622	0.429/26.45	
SCPBB@Cu-0.5	0.999	120.8/0.5	/	10	1.1089	0.282/25. 42	
SCPBB@Ni-0.5	0.997	/	145.4/0.5	10	1.1324	0.297/26.24	
SCPBB	2.143	/	/	/	/	0.504/23.51	

2.3. Materials characterization

The XRD patterns were recorded in the 20° ≤ 2θ≤ 80° range, using a D8 Advance Bruker diffractometer (Cu Kα radiation) with X-ray generator voltage of 40 kV and the current of 40 mA. The step size and scan rate were set to 0.33 ^{o}C and 1.11 $^{o}C.s^{-1}$, respectively. The data were processed using Highscore Plus software.

XPS spectra were recorded using a K Alpha+ apparatus (Thermo, East Grinstead, UK). The machine is fitted with a mono Al Kα (source energy = 1486.6 eV), and a flood gun for charge compensation build-up. The pass energy was set to 200 eV to record the survey spectra and 80 eV for the acquisition of the narrow regions. Avantage software version 5.9902 was used for data acquisition and processing.

Raman spectra analysis was conducted by a Horiba HR 800 instrument to determine the carbon signature at a wavelength of the He−Ne laser beam set to 633 nm. The spectra were acquired in the 800–2700 cm^{-1} region.

We have employed a Hitachi SU 8030 Scanning Electron Microscope (SEM) for imaging the surface morphology, and ZEISS Gemini SEM 360 for the observation of the sample morphology and elemental mapping, respectively. No charge compensation was used, and the source-sample distance was set at 4.2 mm. ImageJ software was used for SEM image processing.

Thermal gravimetric analyses (TGA) were conducted using a Setaram machine Setsys Evolution model to measure the mass loss kinetics of biochar (with or without metallic nanoparticles). The experiments were performed under air atmosphere, over the temperature range RT-800 °C, and setting the heating rate to 10 °C/min.

The chemical composition of the prepared materials were analyzed using the Panalytical MINIPAL4 X-ray fluorescence (XRF) spectrometers analysis with a rhodium X-ray tube operating at 30 kV and 87 μA current emission.

2.4. Catalytic activity investigation

Catalytic tests were performed in a similar manner previously reported by some of us (Omiri, Snoussi et al. 2022). Typically, in each experiment, 5 mg biochar catalyst was added to the dye solution (20 mL, concentration of 0.01 mmol/L). H_2O_2 was added to initiate the Fenton-like degradation reaction of the dye. A similar method has been used to study the degradation of dye mixtures. The suspension was filtered to determine the remaining dye concentration, using UV-Vis spectrophotometry at specific time intervals.

The degradation ratio was calculated using the following formulae:

$$\% \text{ degradation efficiency} = ((C_0 - C_t)/C_0) \times 100, \quad (1)$$

where C_t and C_0 are the concentrations of dye solution at time = t and t = 0, respectively.

Based on the experimental data, the kinetic analysis of dye degradation are fitted according to the following zero-order equation (equation 2) and pseudo-first-order (equation 3) reaction kinetic model (equation. 2) equation:

$$C_t/C_0 = -K_0t \quad (2)$$

$$- \ln(C_t/C_0) = - \ln(A_t/A_0)=K_1t, \quad (3)$$

where A_t and A_0 are the absorbance of the dye at time t and time t= 0 min, respectively. K_0 and K_1 are the zero-order constant and first-order constant, respectively; t is the treatment time.

2.5. Recycling experiment

After the catalytic reaction was completed, the SCPBB@CuNi nanomaterials were separated from the solution by an external magnetic field without any washing, and then reused.

3. Results and Discussion

3.1. General aspects

In previously published reports on biochar@CuNi, the focus has been on the method of preparation and catalytic activity of the designed biochar composites obtained from olive stones in environmental remediation (Khalil, Michely et al. 2021, Omiri, Snoussi et al. 2022) and pistachio shell or pomegranate peels for catalyzing organic chemical reactions (Zarei, Mohammadzadeh et al. 2022, Zarei, Saidi et al. 2022). Herein, we investigate the effect of CuNi bimetallic nanoparticle loading on the dispersion and catalytic activity of the final biochar@CuNi. Moreover, we have employed sugarcane pulp bagasse as a biomass for making biochar, which is rather not explored in the literature compared to the total sugarcane bagasse. The sugarcane bagasse was dried after juice making and scratched in order to obtain the dried pulp bagasse. The latter was further ground, impregnated with metal ions, and pyrolyzed.

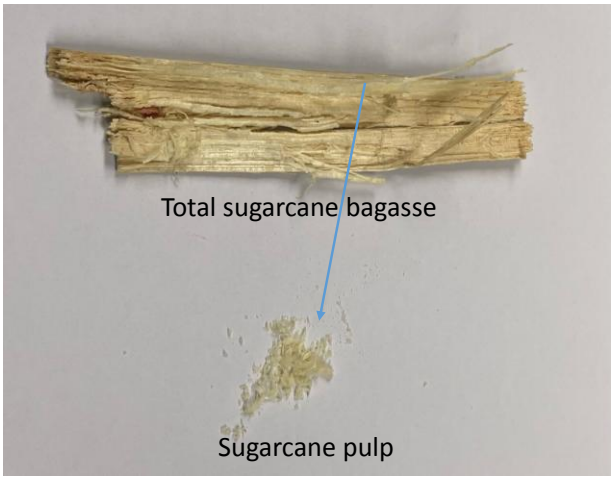

Figure 2. Digital photographs of total sugarcane bagasse, and the pulp obtained after scratching.

3.2. SEM /EDX study

The SEM micrographs of bare and NP-coated biochar are shown in Figure 3. The biochar SCPBB@CuNi-0.5 (Figure 3 a-d) is observed at various magnifications; it forms the ordered arrangement with uniform pores, similar to fishing net. The pores are elongated, almost like slits with length in the 3 to 12 µm range and ~1 µm slit

width (Figure 3a). The pores are of smaller size, which is ascribed to dehydration of the cell structure. Nanoparticles are visible in Figure 3b but are very well distinguished in Figure 3c, which is at a higher magnification. The NPs are densely and homogenously dispersed over the surface, without any evidence of aggregation. This conforms again with our previous findings on CuNi bimetallic NPs loaded on olive stone powder biochar (Khalil, Michely et al. 2021). The protocol is therefore very well reproducible and yields similar results on a different biomass (herein sugarcane pulp bagasse). From Figure 3d, one could estimate the average CuNi nanoparticle size to 40±3 nm, meaning that the bimetallic nanoparticles are in the nanoscale regime (< 100 nm). Oppositely, the SCPB-derived biochar exhibits an almost featureless surface (Figures 3 e-g), with only fewer micrometer-sized pores. The latter seem to be at the origin of the slits displayed by the composite nanomaterials. It further follows that the activation of the biomass with copper and nickel nitrates favours the formation of slits and the highly porous structure, without using any harsh acidic or basic media. At this stage, it is important to note that neither olive pit (Khalil, Michely et al. 2021), nor pomegranate (Zarei, Saidi et al. 2022) biochar loaded with CuNi exhibited such a fishing net-like structure.

Figures 3 (h-k) shows the SEM images of SCPBB@CuNi biochar prepared with various metal ion loading. The porous structure has been changed, showing even smaller pores at higher nanoparticle loading. For SCPBB@CuNi-2, it was difficult to find any porous structure as the one noted for SCPBB@CuNi-0.5. Moreover, at high metal ion loading during the impregnation stage, the pyrolysis process led to substantial agglomeration of CuNi NPs all over the SCPBB surface. A higher content of nanoparticles aggregated on the biochar substrate, leading to possible lower surface area.

SCPBB@Ni-0.5 and SCPBB@Cu-0.5 surface morphologies could be compared in Figures 3 l-o. The SEM images of SCPBB@Cu-0.5 showed just a few pores on the featureless surface, and copper nanoparticles appear flower-shaped. In contrast, SCPBB@Ni-0.5 nanocomposite morphology is almost identical to that obtained with

SCPBB@CuNi. One could then argue that the formation of the highly porous structure is attributed to the addition of nickel, which is known to catalyze the transformation of sp^3 to sp^2 carbon as well as it catalyzes the formation of the porous structure by consuming carbon (Li, Zhao et al. 2021). These structural characteristics could hypothesize the catalytic enhancement due to the fishing net-like structure of SCPBB@CuNi, which exhibits abundant adsorption sites for removing organic pollutants.

Additionally, EDX mapping confirmed the presence of all the desired elements of the SCPBB@CuNi sample at the surface in EDX spectra. Figure 4 shows that SCPBB@CuNi mainly contains C, O, Cu, and Ni, which accounts for the effective loading of copper and nickel on the surface of biochar SCPBB through the simple wet impregnation method. Moreover, the elements simultaneously present in the biochar SCPBB correspond to the C, O, N, Ca, Mg, and Si peaks. The results of EDX analysis were confirmed by analyzing different regions (Table 2); the ratio of Cu/Ni is almost 1:1 with an atomic ratio of 3.66 and 3.56 % copper and nickel, respectively.

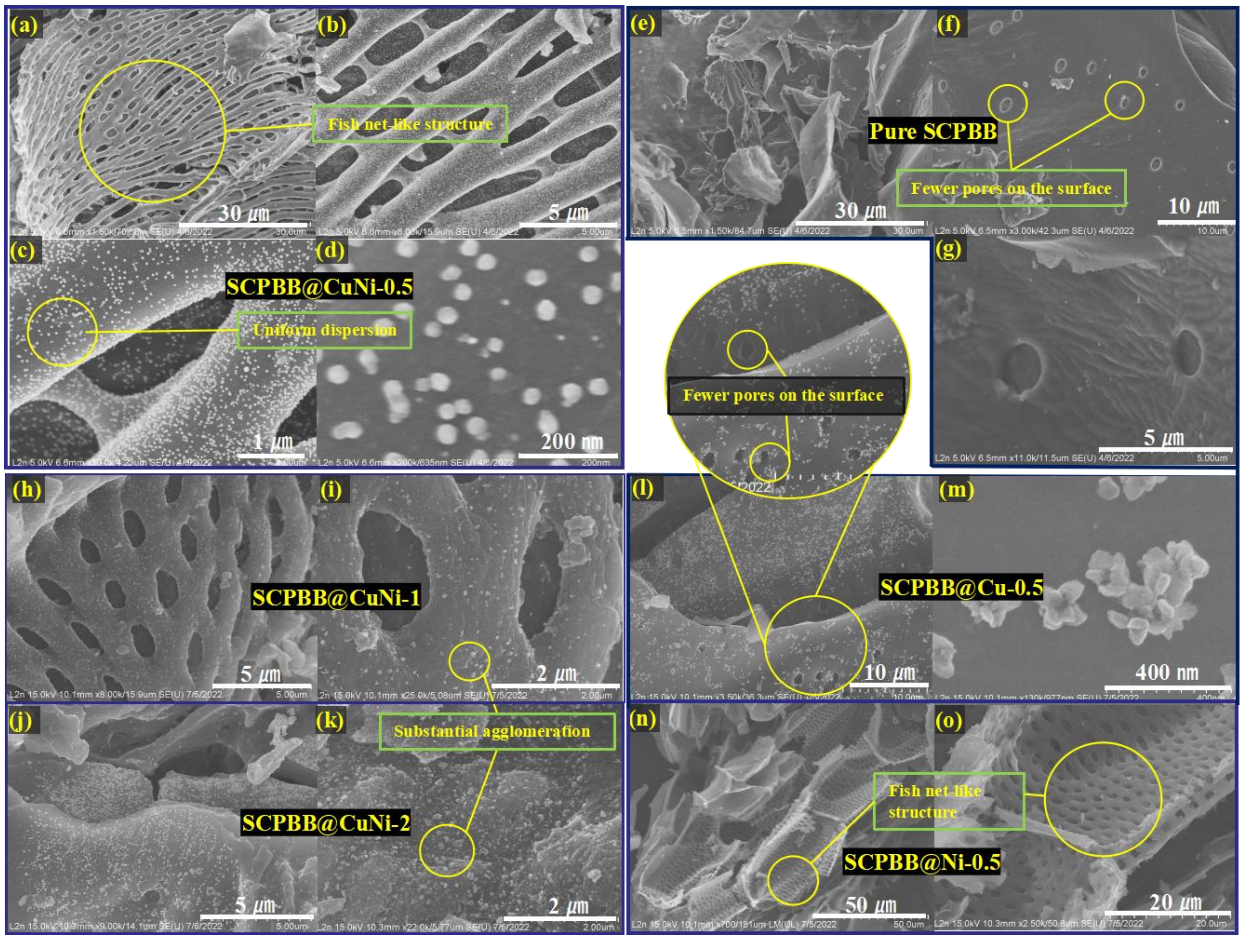

Figure 3. SEM images of SCPBB@CuNi (a-d), SCPBB (e-g) SCPBB@CuNi-1(h,i), SCPBB@CuNi-2 (j,k), SCPBB@Cu (l,m) and SCPBB@Ni (n,o) at various magnifications.

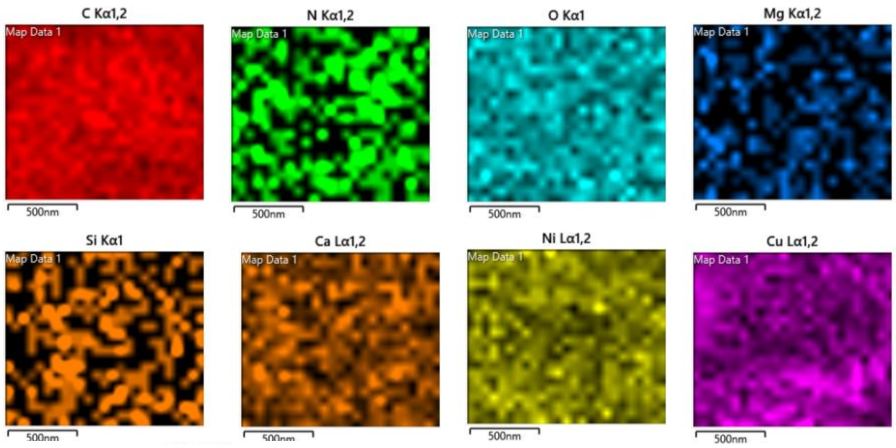

Figure 4. Chemical mapping of SCPBB@CuNi-0.5 at the spots probed for the acquisition of EDX spectra.

Table 2. EDX-determined surface elemental analysis of SCPBB@CuNi-0.5 catalyst.

Catalyst	Elemental Atomic %									
SCPBB@CuNi-0.5	C	N	O	Mg	Si	P	S	Ca	Ni	Cu
	81.39±4.31	0.30±0.4	10.14±2.19	0.14±0.4	0.36±0.29	0.08±0.02	0.11±0.01	0.23±0.05	3.56±0.17	3.66±2.46
	Weight %									
	Cu		Ni		O	Mg	Si	P	S	K
	31.25±0.25		31.91±0.26		29.71±0.19	0.73±0.07	2.50±0.09	0.40±0.10	0.46±0.13	3.04±0.34

3.3. XRD

The XRD analyses were conducted on bare SCPBB, and copper and nickel nitrate-impregnated biochar. As shown in Figure 4a, it is worth noting that there is no corresponding diffraction peak for SCPBB after biomass calcination. The diffraction peak exhibited by SCPBB@Cu at 50.7 ^{o} corresponds to the Cu(111) reflection planes of Cu^{0} species (ICSD 98-0050-3757), whereas the diffraction peak at 51.9 ^{o} exhibited by SCPBB@Ni is attributed to the Ni(111) reflective surface of the Ni^{0} species (ICSD 98-007-6667). The diffractogram corresponds to SCBPP@CuNi and reference biochar in Figure 4b. The XRD pattern does not show any single metal copper or nickel, and two new diffraction peaks are displayed at 51.5 ° and 59.8 ° are assigned to structures of copper and nickel metals (111), (002) crystallographic planes, respectively (ICSD 98-062-8543). In addition to the Cu peak, Cu_2O also appears at 2θ = 42.3°. This indicates that SCBPP@CuNi showed the presence of a crystalline structure of copper-nickel alloy on biochar.

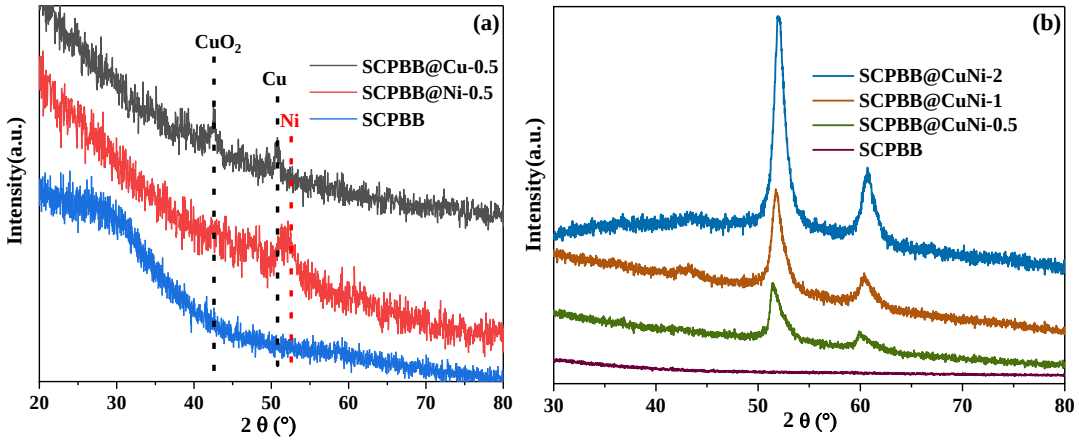

Figure 5. XRD patterns of SCPBB, SCPBB@Cu and SCPBB@Ni (a); and SCPBB@CuNi composites at various CuNi loadings (b).

3.4. XPS surface chemical analysis

XPS was employed to investigate the surface chemical composition of biochar and its nanocatalyst-decorated counterparts. Figure 6 displays the survey spectra of bare SCPBB (Figure 6a) and the SCPBB@CuNi samples (Figures 6b-d). Cu2p and Ni2p are very clearly visible and account for the fine dispersion of the nanoparticles as imaged by SEM. Interestingly, one could note the gradual increase in the relative Cu2p and Ni2p peak intensity versus the initial impregnation rate of the biomass with the metal nitrates. Concerning the monometallic nanocatalyst systems, the survey spectra are displayed in Figure 6e and Figure 6f for SCPBB@Ni and SCPBB@Cu, respectively. In either the mono- or the bimetallic system, XPS testifies for the presence of these elements in the metallic states as noted in the inset of Figure 6a-d ($Ni2p_{3/2}$ at ~852.1 eV; sharp $Cu2p_{3/2}$ peak centred at 932.1 eV). The $Cu2p_{3/2}$ spectrum has two overlapping features at 932.7 and 934.4 eV, assigned to Cu^0 and CuO, respectively (Biesinger 2017). In addition, small shake-up satellites are located in the 938-948 eV region, indicating the presence of Cu^{2+} species in the SCPBB@CuNi (Jha, Jeong et al. 2015, Biesinger 2017). The $Ni2p_{3/2}$ narrow region exhibits a sharp peak at 852.7 eV, and a broad region at 854-861 eV attributed to Ni and nickel oxides, respectively. The binding energy values reported for metallic copper and nickel in the alloy fit in well with those reported by the NIST XPS database

(https://srdata.nist.gov/xps/) for pure copper and nickel, taken separately. Probably, this is due to the equal electronegativity of copper and nickel (~1.9). Elsewhere, no major shift was found for CuNi compared to pure copper or nickel (Wolfbeisser, Kovács et al. 2017).

Table 3 reports the apparent surface composition determined by XPS for the biochar and the corresponding mono- and bimetallic systems. A few trends could be noted from the data reported in Table 3: (i) there is a monotonous increase in the (Cu+Ni)/C atomic ratio versus the total initial impregnation rate, defined as the total number of metal salt millimoles per gram of sugarcane pulp bagasse (Figure 6g). Interestingly, the monometallic system fits in well with the plotted data for the bimetallic system, which rules out any synergetic effect of copper and nickel on the (Cu+Ni)/C atomic ratio. This chemical descriptor accounts for the gradual changes in the surface morphology as imaged by SEM. (ii) Moreover the N/C atomic ratio increases monotonously with the initial impregnation rate.

N/C atomic ratio could be considered a chemical descriptor of the nitrogen-doping of the carbonaceous structure. It could be due to the nickel catalytic effect resulting in the loss of carbon, which led to the biochar porous structure (see above, section 3.2). The increase in N/C could also be due to the nitrates as a nitrogen source for doping the carbonaceous biochar structure. Elsewhere, ammonium nitrate impregnation was reported to induce nitrogen doping of the biochar (Kasera, Kolar et al. 2022).

Table 3. XPS-determined surface chemical composition of biochar samples

Materials	C	O	N	Ni	Cu
SCPBB	84.6	14.9	0.5	-	-
SCPBB@CuNi-0.5	81.6	15.8	1.37	0.31	0.65
SCPBB@CuNi-1	82.3	13.3	2.30	0.71	1.44
SCPBB@CuNi-2	79.7	13.4	3.13	1.61	2.11
SCPBB@Ni-0.5	82.6	15.6	1.22	0.46	-
SCPBB@Cu-0.5	81.8	16.3	1.17	-	0.57

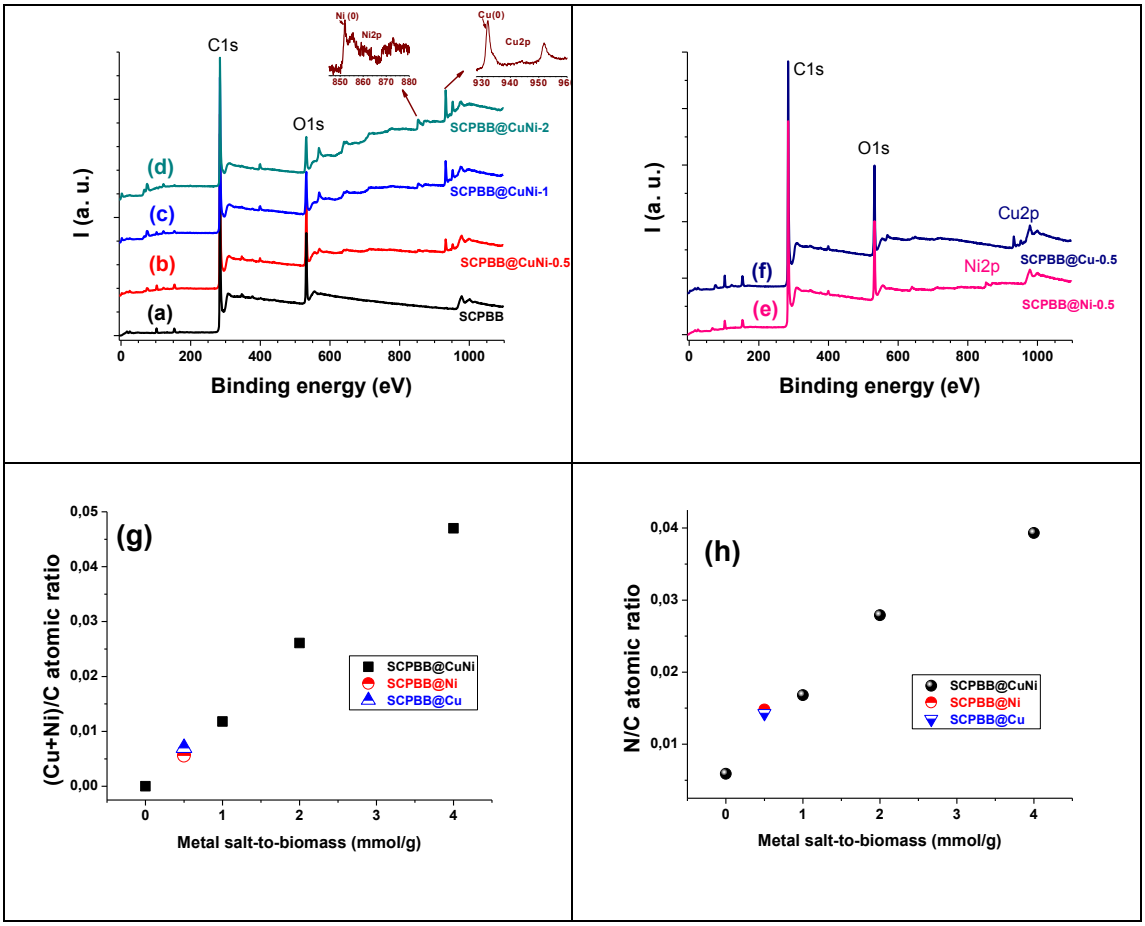

Figure 6. XPS analysis of biochar samples: survey spectra of SCPBB (a), SCPBB@CuNi-0.5 (b), SCPBB@CuNi-1 (c), SCPBB@CuNi-2 (d), SCPBB@Ni-0.5 (e), and SCPBB@Cu-0.5 (f). High resolution Cu2p and Ni2p spectra are shown in inset of Figure 6a-d. Atomic ratios are plotted versus the initial metal impregnation rate in mmol nitrate per gram of biomass: (Cu+Ni)/C (g) and N/C (h).

3.5. Raman characterization of biochar D and G bands

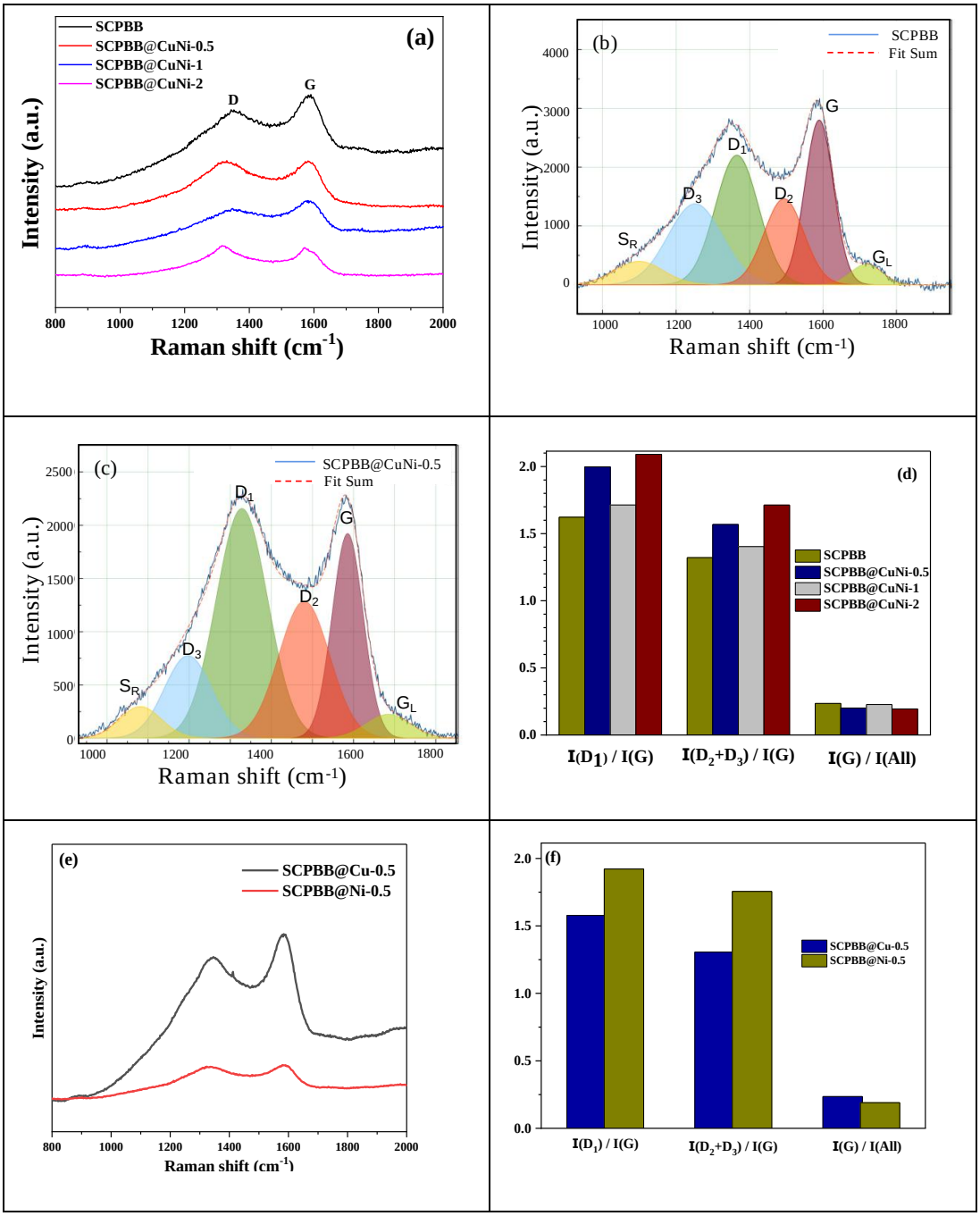

Figure 7. Raman spectra of bare SCPBB biochar and SCPBB@CuNi composites(a), curve-fitted Raman spectra of bare SCPBB biochar(b) and SCPBB@CuNi composites(c), the band area ratio of $I(D_1)/I(G)$, $I(D_2 + D_3)/I(G)$ and I(G)/I(All) obtained from the peak splitting(d), Raman spectra(e) and the band area ratio (f) of SCPBB@Cu and SCPBB@Ni.

To have further insights into the structural transformations of bare SCPBB and to infer the presence of graphitic characteristics (da Silva Veiga, Schultz et al. 2020, Dong, Yang et al. 2021), biochar was characterized by Raman spectroscopy with a 633 nm laser to assess the degree of carbonation of carbonaceous materials (da Silva Veiga, Cerqueira et al. 2021). The spectral curve fitting of Raman spectra from 950 to 1950 cm^{-1} is shown in Figure 7. Six main Gaussian peaks are centred at 1081, 1197, 1328, 1480, 1585, and 1685 cm^{-1}, and assigned to S_R, D_3, D_1, D_2, G, and G_L bands, respectively (Li 2007, Cao, Yuan et al. 2021). The peak of SR at 1081 cm^{-1} is attributed to the C–H on aromatic rings, and the D band centered at 1328 cm^{-1} referred to disorder and defective carbonaceous material, and aromatics with not less than 6 benzene rings. The G band mainly represents aromatic ring quadrant breathing with graphite E_2g_2 structures. The D_2 centred at 1480 cm^{-1} is mainly attributed to the semi-circle breathing of aromatic rings and amorphous carbon structures (Cao, Yuan et al. 2021). The SR and D_3 bands can be ascribed to the C–H on aromatic rings and the aryl–alkyl ether. The broad G_L band originated from the carbonyl group of biochar catalysts.

There is a significant change of D-G doublet with the loading of copper and nickel; D/G becoming higher than 1 (NB: peak area ratio, and not peak height ratio is considered), thus indicating that loading nanoparticles onto the biochar may impede the formation of the graphitic structure of the biochar during pyrolysis (Cao, Yuan et al. 2021, Sun, Feng et al. 2022)**.** The evolution of catalysts crystalline structure was investigated using band area ratios $I(D_1)/I(G)$, $I(D_2 + D_3)/I(G)$, and $I(G)/I(All)$, as displayed in Figure 7d. The $I(D_1)/I(G)$ ratio and $I(D_2 + D_3)/I(G)$ ratio of SCPBB@CuNi increased consistently compared to pure SCPBB, while the I(G)/I(All) ratio showed a contrasting trend. The results suggested that the concentration of carbon structures (not less than 6 benzene rings) containing defects and heteroatoms increases as a result of the dehydrogenation of hydroarenes (Cao, Yuan et al. 2021). As far as the monometallic systems are concerned, $I(D_1)/I(G)$, $I(D_2 + D_3)/I(G)$, and I(G)/I(All) values for SCPBB@Ni-0.5 (Figure 7e,f) match those of SCPBB@CuNi-

0.5, which indicates that nickel only has a profound effect on the carbon structure of the biochar.

3.6. Thermogravimetric analysis of biochar samples

The thermogravimetric (TG) curves for the bare biochar and SCPBB@CuNi are shown in Figure 8a. Thermal analysis was conducted in air to monitor the thermal stability and determine the mass loading. These curves show the residual weight % of CuNi-decorated biochar is higher than that of SCPBB at a high temperature; the weight loss of SCPBB is about 90% at 800 °C. Adding copper and nickel to biochar resulted in a significantly higher residual weight %, which accounts for the initial metal ion loading at the wetness impregnation step before pyrolysis. Copper and nickel from the bimetallic NPs convert to metallic oxides, hence SCPBB@CuNi yields slightly higher weight % due to oxygen in CuO and NiO. Similarly, the residual weight % of SCPBB@Cu-0.5 and SCPBB@Ni-0.5 are higher than those of pure biochar but lower than that of SCPBB@CuNi-0.5. There is clear control over the preparation procedure adopted in this work for the fabrication of biochar loaded with bimetallic nanocatalysts.

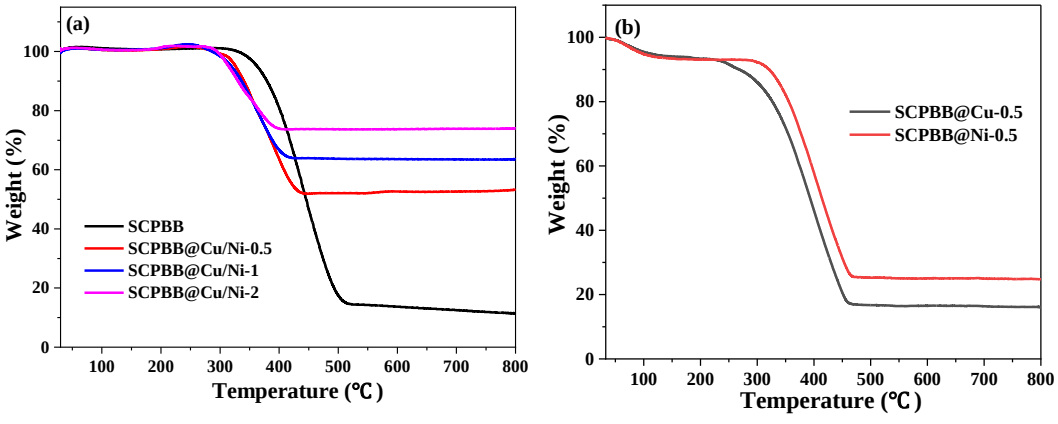

Figure 8. TG curves of SCPBB and SCPBB@CuNi samples (a), SCPBB@Cu-0.5 and SCPBB@Ni-0.5 (b). Analysis in air; heating rate = 10 °C min^{-1}.

3.7. Catalytic oxidation of dye solution using biochar@CuNi

3.7.1. Removal of single dyes from aqueous solutions

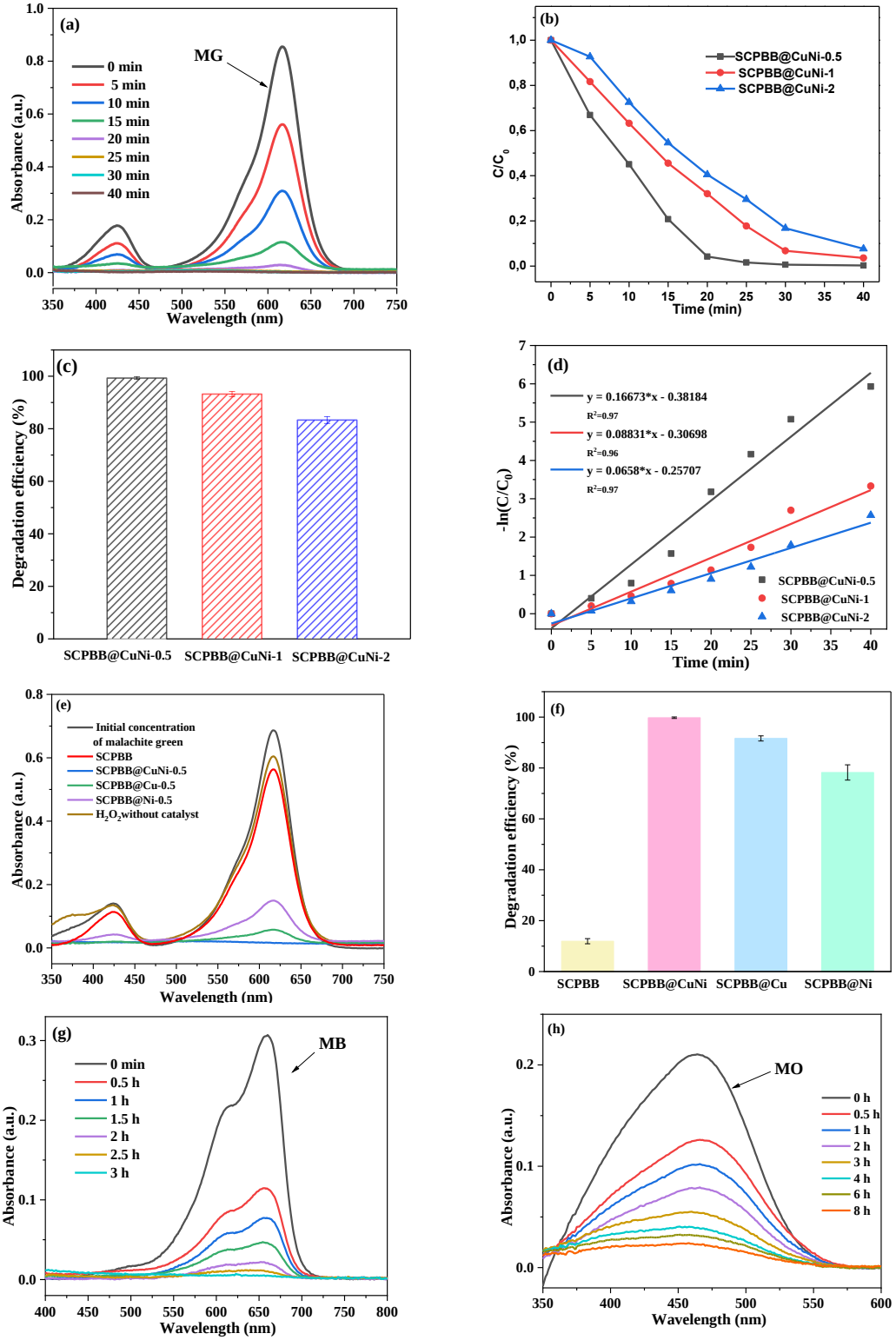

Figure 9. UV-vis spectra of dye solutions during the catalysis degradation reactions of Malachite Green (a), Methylene Blue (g), and Methyl Orange (h). C/C0-*vs*-time plots for MG degradaed using biochar@CuNi catalysts (b) and the corresponding removal % after 30 min (c). Pseudo first order kinetic model for MG catalytic reaction with different metal mass loading samples of SCPBB@CuNi (d). UV-vis spectra of Malachite Green dye solutions in 30 min (e), the corresponding removal % after 30 min for Malachite Green dye solutions (f).

Figures 9 (a)–(d) show that the degradation of Malachite Green (MG) dye varied with Cu and Ni loadings. The order of MG dye solution degradation is: SCPBB@CuNi-0.5 > SCPBB@CuNi-1 > SCPBB@CuNi-2, and the degradation efficiency of MG over SCPBB@CuNi 0.5, 1, and 2 nanocomposites in 20 min, was 99.3, 93.2 and 83.3%, respectively. To better understand the kinetic behaviour of different catalysts for MG degradation, the pseudo-first order kinetic model of MG dye removal was applied (Figure 9c). As shown in the linear relationship between time and $-\ln(C/C_0)$; all the prepared samples exhibit good linear correlations, and their R^2 values were close to 1 for SCPBB@CuNi-0.5, 1, 2 nanocomposites. From the above, the degradation activity of metal nanoparticle-doped SCPBB is best obtained for the minimum metal loading, in the decreasing order SCPBB@CuNi-0.5 > SCPBB@CuNi-1 > SCPBB@CuNi-2. This trend accounts for the excellent dispersion of CuNi nanoparticles over the biochar surface when the initial metal ion to biomass ratio is set to 0.5 mmol/1g. It follows that the catalytic activity of the materials prepared so far correlates very well with the state of dispersion of the NPs as observed by SEM.

Subsequently, we further performed the degradation of MG dye in 30 min on pure SCPBB, single metal-supported SCPBB@Cu and SCPBB@Ni, and the presence of H_2O_2 without catalyst in Figures 9(e)-(f). We found that both pure SCPBB and H_2O_2 alone could only remove a small number of dye molecules, whereas the removal efficiencies of SCPBB@Cu-0.5 and SCPBB@Ni-0.5 were 91.6 and 78.2 %, respectively, indicating that copper and nickel played important role in the dye degradation, respectively. Note, however, that SCPBB@Cu-0.5 is more efficient as

Fenton-like composite catalyst than SCPBB@Ni-0.5 (Wang, Ma et al. 2018) (Radji, Bettahar et al. 2022).

The discoloration of single MB and MO with SCPBB@CuNi-0.5 reached 98% and 74% in 3 h, respectively. The complete discoloration of MO occurred after 8 h. The superior activity exhibited by SCPBB@CuNi-0.5 can be attributed to the activation of H_2O_2 by the metallic species loaded on the biochar to generate more hydroxyl radicals, which attack the dye molecules to generate water, dinitrogen, and carbon dioxide (Nidheesh, Gandhimathi et al. 2013, Wang, Sun et al. 2021, Rani, Nayak et al. 2022).

3.7.2. Degradation process of mixed dye solutions

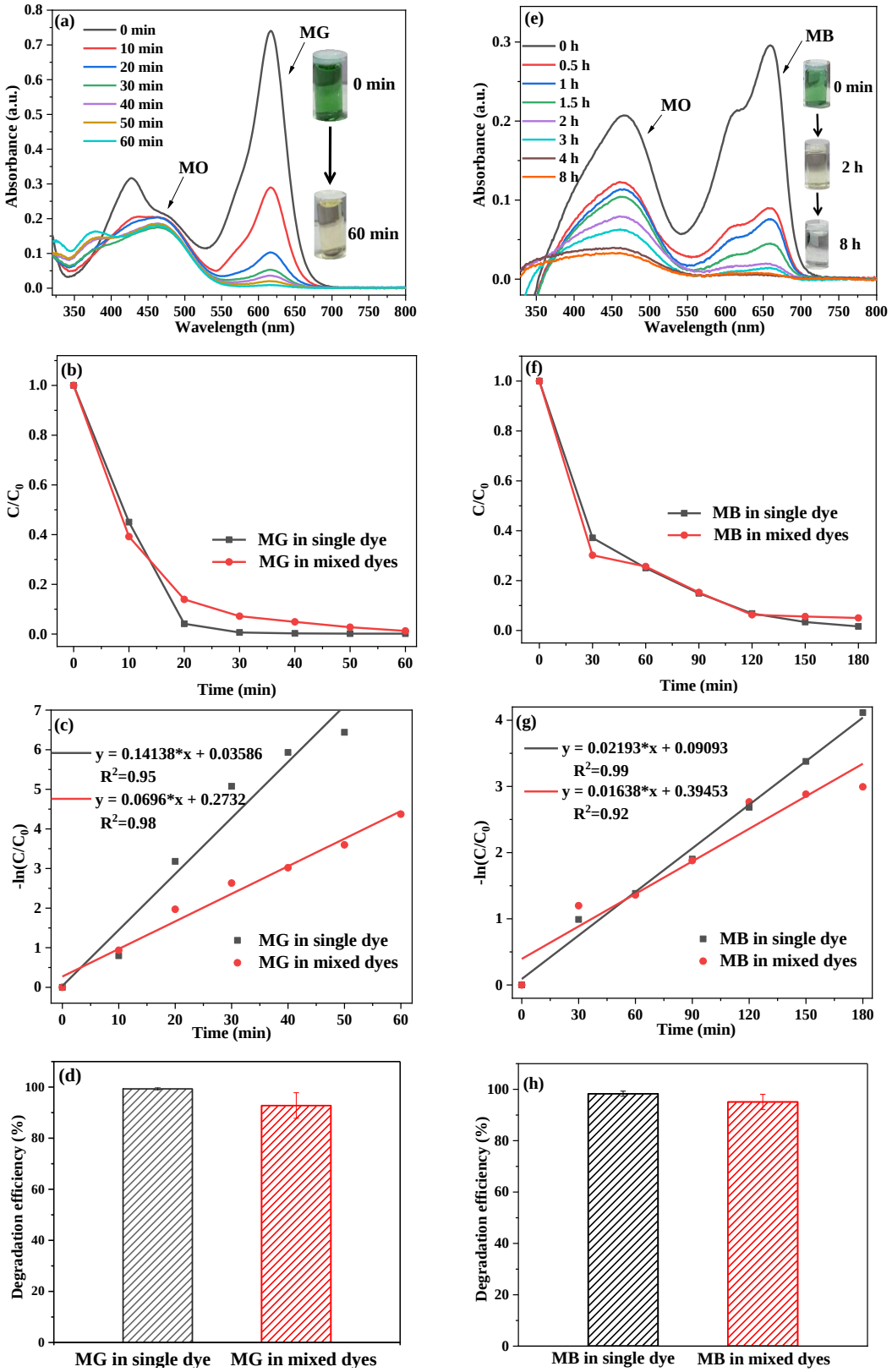

Figure 10. (a) UV-vis spectra, (b) degradation, (c) Pseudo first order kinetic model and (d) degradation efficiency for simultaneous degradation of binary mixture of dyes MO and MG, (Ⅰ) MG change of individual dye, (Ⅱ)MG change of multiple dyes. (e) UV-vis spectra, (f) degradation, (g) Pseudo first order kinetic model and (h) degradation efficiency for the binary mixture of dyes MO and MB, (Ⅲ) MB change of individual dye, (Ⅳ)MB change of multiple dyes. Operation condition: MG initial concentration= 0.02 mmol/L, MB initial concentration= 0.02 mmol/L, MO initial concentration= 0.02 mmol/L, biochar dosage = 0.25 g/L.

Preliminary tests showed that SCPBB@CuNi-0.5 could optimally degrade individual dye solutions under natural light in the presence of H_2O_2, which prompted us to study its catalytic performance for mixed dyes. Recently, some of us have tried to study brewer's spent grain Biochar@Ag-Cu for Methyl Orange and Methylene Blue mixed dye solution, and the degradation rates were excellent after 6 hours (Boubkr, Bhakta et al. 2022). For this study, two different types of equimolar dye mixtures (MG+MO and MB+MO mixtures) were prepared to understand how the SCPBB@CuNi catalyst would still maintain the significant degradation rate of single organic dye pollutant in complex binary dye solutions.

After the selective degradation spectra of the two mixtures were established using the same conditions, the catalytic degradation reaction of the three dyes MG, MB, and MO (equimolar mixture) with the catalyst was investigated, and then compared with the degradation performance in the corresponding single dye systems. As shown in Figure 10a, MG dye in the MG+MO mixture showed an obvious sharp decrease to completely disappear at 616 nm, the absorbance drop of MO at 464 nm was very slight; the mixture's color gradually changed from green to yellow after 60 min. It took longer for MO to completely degrade.

In the MB+MO system, we have also noted faster degradation of MO, thus leading to a change of color from green (MB+MO mixture) to light yellow due to complete degradation of MB while there were persistent MO molecules in the solution. Complete discoloration of the MB+MO system was reached after 8 h. The

degradation rates of MB and MO were 95% (after 3 h) and 84% (after 8 h), respectively.

In addition, the degradation rate and first-order reaction kinetics of SCPBB@CuNi in the single dye solution and dye mixture system are also explored. The C/C_0-vs-time plots for MG and MB dye degradation in mixed dyes using SCPBB@CuNi catalyst are shown in Figure 10(b,f): faster degradation of the dye solution occurs during the first 30 minutes (Rani, Nayak et al. 2022). We found that the degradation rate of an individual dye in the mixed solution was slightly reduced within 5% and the kinetics versus reaction time plot clearly showed that all MG degradation processes followed a pseudo-first-order kinetic model (linearization coefficient $R^2 > 0.90$). The SCPBB@CuNi catalyst retains its performance in the degradation of the dyes, and the dye mixtures do not seem to significantly alter its efficiency.

3.7.3. *Mechanism*

The plausible dyes degradation mechanism by the catalytic oxidation of SCPBB@CuNi/H_2O_2 system follow adsorption and Fenton-like reactions (Liu, Liu et al. 2022). Its characterizations confirmed the particular pore structure, graphitic carbon, and metallic states of copper and nickel loaded on the underlying biochar. Heterogeneous Fenton-like reactions played a dominant role in the catalytic degradation process, and adsorption played a minor role in dye removal. The bimetallic species loaded on the biochar in SCPBB@CuNi provided active sites for activating H_2O_2 to generate hydroxyl radicals (Liu, Liu et al. 2022). SCPBB created an excellent support for metallic species. In order to further understand whether metal leaching from catalyst into the solution causes secondary pollution, the loss of metal copper/nickel was detected by XRF technology. Firstly, the XRF analysis of the carbonaceous catalyst SCPBB@CuNi-0.5 showed that the alloy represents $\approx$ 13.7 % from the total mass. Also, it revealed that Cu alone represents $\approx$ 93% from the total mass of the alloy. For catalytic performance testing, we used 5 mg of catalyst

containing 685 ng CuNi, 637 ng Cu, and 48 ng Ni. After completing the catalyzed reaction under natural light, no copper and/or nickel leaching into the solution were observed by XRF technique, meaning their absence from the solution, or their quantity is below the detection limit of the apparatus. This is strong supporting evidence that either metal lixiviation was negligible or did not occur at all from the catalyst. One could thus conclude that heterogeneous Fenton-like catalysis reaction dominates the whole process. For this reason, the catalyst surface does not undergo significant surface chemical composition, retains its active sites, therefore ensuring high catalytic performances (Soon and Hameed 2011, Liu, Jiang et al. 2022). Robust anchoring of the CuNi nanoparticles is essential, and this point will be tackled below (see section 3.9). Meanwhile, organic pollutants can be completely mineralized into carbon dioxide and water, simultaneously, elucidating that dye degradation mainly ascribe to surface catalysis of heterogeneous Fenton-like reactions rather than homogeneous Fenton-like reactions in solution (Xavier, Gandhimathi et al. 2015). Under H_2O_2 conditions, pH effect was reported to be crucial for the control of the catalytic activity(Bokare and Choi 2014). Particularly, both copper/H_2O_2 (Radji, Bettahar et al. 2022) and nickel/H_2O_2 (Akram, Ikhlaq et al. 2021) systems are active over a broad pH range.

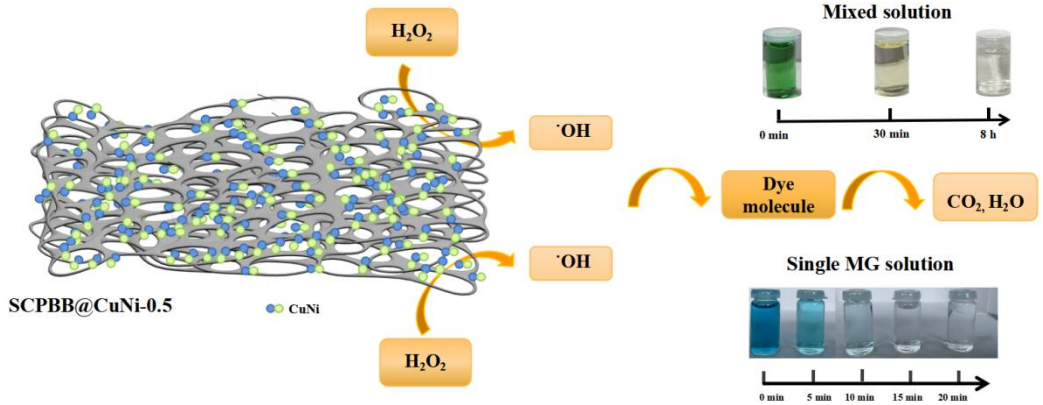

Fig. 11. Proposed possible reaction mechanism for dye degradation in SCPBB@CuNi/H_2O_2 system.

Therefore, based on these results, SCPBB@CuNi can effectively degrade individual dye solutions and mixtures with H_2O_2 may be attributed to the following

aspects: (1) The special fishnet-like porous structure of substrate SCPBB material is easy to adsorb, resulting in dye molecules being concentrated around the metal nanoparticles to increase their degradation. (2) More hydroxyl radicals and metal ions are produced to attack the dye molecules, which are mineralized into carbon dioxide and water to achieve discoloration.

In summary, the whole process of Fenton-like degradation could occur through the following pathways.

Dye molecule + SCPBB@CuNi → D-SCPBB@CuNi (4)

Biochar and metal ions in the catalyst accelerate the generation of hydroxyl radicals, as shown in the following formula (Wang, Liu et al. 2021)

$Cu^{+} + H_2O_2 \rightarrow Cu^{2+} + {}^{\bullet}OH + OH^{-}$ (5)

$Cu^{2+} + H_2O_2 \rightarrow Cu^{+} + HO_2^{+\bullet} + H^{+}$ (6)

Degradation of dye solution via the attack of the hydroxyl radicals plays the dominant role in dye solution discoloration.

D-SCPBB@CuNi+ $^{\cdot}OH$ → colorless degradation products (7)

Similarly, nickel could participate in the Fenton-like degradation of the dyes. As suggested, by Bhaumic *et al.* (Bhaumik, Maity et al. 2022):

$Ni^{0} + 2H_2O \rightarrow Ni^{2+} + {}^{\bullet}H_2 + 2OH^{-}$ (8)

$Ni^{2+} + H_2O_2 \rightarrow Ni^{3+} + OH^{-} + OH^{\bullet}$ (9)

$OH^{\bullet}$ + dyes → colorless degradation products (10)

If the role of copper is restricted to catalysis only, nickel has dual properties: catalysis and magnetic properties that permits collection of the biochar with a magnet, after use.

3.8. Comparison with other biochar-based catalytic systems

Table 4 compares the catalytic performance of SCPBB@CuNi to other biochar-based systems.

Table 4. Comparison of the catalytic performances of SCPBB@CuNi to other biochar-base materials.

Catalyst	**Experimental conditions**	**Contact Time(min)**	**Degradation (%)**	Recovery **(cycle times, degradation)**	**References**
		Malachite Green			
Mn/SRBC (KMnO4/ biochar)	Catalyst 2 g/L, H_2O_2 5 m mol/L, MG 8000 mg/L, pH 3, temperature 30°C	90	100	3rd cycles, 62%	(Zhu and Zou 2022)
PBC@δ-MnO_2	Catalyst 0.2 g/L, PDS 1 mmol/L, pH 5, MG 200 mg/L, temperature 30 °C	120	92.6	4th cycles 75%	(Xia, Li et al. 2023)
BMFH/Fe_3O_4	Catalyst 1.0 g/L, MG 50 mg/L, H_2O_2 50 mmol/L, pH 6, temperature 30 °C	60	99	10 cycles 81%	(Chen, Lin et al. 2022)
Fe@BCFAK	Catalyst 0.2 g/L, MG 20 mg/L, H_2O_2 2 mmol/L, pH 3, temperature 30 °C	30	98	/	(Xia, Shen et al. 2022)
Fe NPs/tea extract	Catalyst 50 mg/L, MG 50 mg/L, H_2O_2 7.4 mmol/L, pH 4, temperature 35°C	60	78.2	/	(Wu, Zeng et al. 2015)
ZnO@BC	Catalyst 0.4 g/L, MG 400 mg/L, 300 W xenon lamp (no mention)	60	98.4	/	(Jing, Ji et al. 2021)
Algal biochar@La/Cu/Zr	Catalyst 0.4 g/L, MG 2×10^{-6}mmol/L, solar light	240	90	4 cycles 71%	(Sharma, Bhogal et al. 2019)
$CuFe_2O_4$@biochar	Catalyst 0.2 g/L, PS 2.5 mmol/L, MG 100 mg/L, pH 8, temperature 55°C	90	98.5	5 cycles 90%	(Huang, Chen et al. 2021)
SCPBB@CuNi	Catalyst 0.25 g/L, H_2O_2 48 mmol/L, MG 9.3 mg/L, room temperature	30	>99	4 cycles 87±3%	This work

Methylene Blue					
BGT-NPs	Catalyst 0.25 g/L, H_2O_2 16 mmol/L, MB 10 mg/L, UV-light, wide pH range	120	96−99%	4 cycles 96%	(Ashraf, Rasool et al. 2021)
P-GBC (H_3PO_4 activation)	Catalyst 0.1 g/L, H2O2 0.2 mmol/L, PMS 4 mmol/L MB 100 mg/L, temperature 298.15 K	360	94.9%	3 cycles 79%	(Ding, Tong et al. 2023)
MnO_2@SBC	Catalyst 0.3 g/L, pH 7 PMS 0.5 mmol/L MB 35 mg/L, temperature 25 °C	180	100%	5 cycles 0.02084 min_{-1} (degradation rate)	(Li, Liu et al. 2022)
SCPBB@CuNi	Catalyst 0.25 g/L, H_2O_2 4.8 mol/L, MB 3.2 mg/L, room temperature	180	>98%	/	This work
Methyl Orange					
H_2SO_4 biochar	Catalyst 1 g/L, H_2O_2 25 mmol/L, MO 50 mg/L, 1000 W Xe arc light temperature 50 °C;	60	92%	5 cycles >80%	(Rangarajan and Farnood 2022)
Biochar@Cu_2O	Catalyst 0.1 g/L, MO 20 mg/L, UV light, pH 4, temperature 50 °C;	140	94.5 %	/	(zhang, Li et al. 2023)
SCPBB@CuNi	Catalyst 0.25 g/L, H_2O_2 4.8 mol/L, MO 3.2 mg/L, room temperature	480	>90%	/	This work

BCFAK acid-precipitated black liquor of poplar kraft pulp ; BMFH magnetic biochar fungal hyphae *(Trichoderma reesei) ;* PBC the phosphoric acid modified millet husk biochar; P-GBC P-GBC was prepared by H_3PO_4 assisted pyrolysis over camellia shell powder; PMS: peroxymonosulfate PMS; SRBC spirulina residue biochar.

Concerning the degradation of MG, the biochar composites catalysed the removal of MG with efficiency in the 78–99 wt.% range, within 30 to 240 min. It is worth noting that, under natural pH conditions, the degradation of dyes remains difficult. The degradation efficiency of Fe@BCFAK (Xia, Shen et al. 2022) and Mn/SRBC (Zhu and Zou 2022) is over 98% within 60 minutes, which is very similar to SCPBB@CuNi, but under acidic pH. The ZnO@BC catalysed the removal of MG within 60 min under xenon lamp irradiation (Jing, Ji et al. 2021). The actual SCPBB@CuNi/H_2O_2 system catalyzed the removal of MG cationic dyes to an extent of 99% within 30 min only, under natural light and neutral pH. In addition, no acidic or alkali treatment was applied to obtain highly porous biochar.

Magnetic biochar (BMFH/Fe_3O_4) (Chen, Lin et al. 2022) was synthesized by the bio-assembly property of fungal hypha; the removal rate of MG remained above 80% after 10 cycles, but the catalyst was washed and carbonized before the next cycle.

The degradation performance of $CuFe_2O_4$@biochar is always maintained at 90% after five reactions (Huang, Chen et al. 2021). The catalyst/PS system also possesses promising prospects for treating wastewater. Even if four-time reactions, compared with the PBC@δ-MnO_2 (Xia, Li et al. 2023) and Algal biochar@La/Cu/Zr (Sharma, Bhogal et al. 2019) catalysts, the degradation performance of SCPBB@CuNi was found to be as high as 87% after four cycle tests, no washing and drying steps were done and the catalyst was directly re-used for a new catalysed degradation. This is of practical application importance.

Concerning the Fenton-like process, the literature reported large amounts of H_2O_2, or extra oxidants or light irradiation could significantly improve the effect of the catalytic system, which contrasts with our much simpler conditions consisting in using low H_2O_2 amounts, under daylight exposure. Ashraf *et al.* (Ashraf, Rasool et al. 2021) on the one hand, and Rangarajan *et al.* (Rangarajan and Farnood 2022), on the other hand, used UV light source to the catalyst/H_2O_2 system to increase the degradation rate of the dye. P-GBC (Ding, Tong et al. 2023) and MnO_2@SBC (Li, Liu et al. 2022) catalytic systems were combined with peroxymonosulfate (PMS), as an alternative to H_2O_2 to produce active species. To further know whether H_2O_2 suffices to remove the dyes and plays a major role in their degradation, reactions were conducted in the absence of catalyst, but the degradation efficiency was only about 30%, with only H_2O_2

and under the same condition. It can thus be confirmed that the degradation rate of MB and MO can reach 98% and 90% only when the catalyst and H_2O_2 coexist.

These dye degradation experiments suggest that SCPBB@CuNi not only has advantages in degrading MG but also has catalytic performance in degrading MB and MO under the synergistic effect of H_2O_2, under daylight.

This comparative study shows that SCPBB@CuNi is a very competitive catalytic composite compared to other biochar-based catalyst systems employed to remove MG, MB, and MO dyes, as well as their mixtures.

3.9. Stability and recovery of the catalyst

Due to the presence of Ni species in the catalyst, after each catalytic reaction, the catalyst was easily separated by an external magnet, and then used for the next catalytic testing, without any washing treatment.

We recollected SCPBB@CuNi-0.5 material by an external magnet to evaluate reusability and stability, without any cleaning treatment, then the catalyst was reused under the same conditions for the MG degradation. Figure 12(a) shows that discoloration occurred at 87±3% and can still be maintained within 20 mins after four times. It is worth noting that the catalyst can be reused without any secondary washing, and retains high catalytic efficiency. This simple recycling method, without any washing step, shows that SCPBB@CuNi is a green and cost-effective catalyst. The crystalline structure of the catalyst after many times of usage was analyzed by XRD (Fig. 12b). Comparing the XRD patterns of the original and the used SCPBB@CuNi catalyst hardly show any significant change, hence the stability of the immobilized bimetallic CuNi NPs.

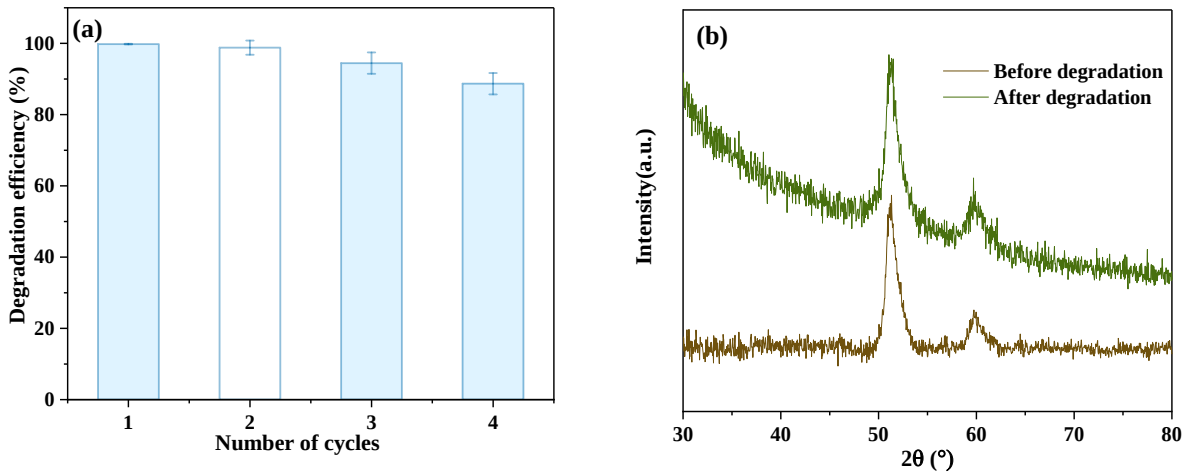

Figure 12. (a) The degradation efficiency of MG dye solution after 4 times with SCPBB@CuNi, (b) XRD patterns of reused and fresh SCPBB@CuNi.

4. Conclusion

In this contribution, sugarcane pulp bagasse biochar samples, loaded with bimetallic copper-nickel alloy nanoparticles, were prepared by pyrolysis at 500 °C, during 1 hour, under dinitrogen stream. SEM images reveal the unusual hierarchical micro/nanostructure resembling to a fishing net, with evenly dispersed and immobilized ~40 nm-sized nanoparticles. The fishnet-like structure of the underlying biochar is shown to be induced by nickel, which also endows the biochar with magnetic properties. Copper and nickel are mostly present in the metallic state but undergo surface oxidation as probed by XPS. Their loading on the biochar gradually increased with initial metal ion impregnation. The unique textural properties and evenly dispersed bimetallic nanoparticles over the optimized biochar SCPBB@CuNi contribute to the superior catalytic activity for removing organic contaminants. The biochar/H_2O_2 system was tested for the degradation of model dyes and their mixtures at RT and under daylight conditions. The SCPBB@CuNi-0.5 catalyzed the total degradation of MG and MB dyes within 30 min and 3 h, respectively, and could be recycled without a significant decrease in its catalytic performance. Even in complex dye mixtures, the catalyst maintained a high ability to remove organic pollutants. For higher initial loading of 1 and 2 mmol metal ions per gram of biomass, the catalytic efficiency decreased due to significant agglomeration of the CuNi nanoparticles.

From the above, this work obviously opens avenues for its application to the treatment of complex wastewaters containing organic pollutant mixtures, therefore contributing to address UNs 6th SDG related to Clean Water & Sanitation.

Acknowledgements.

S. Lau-Truong, P. Decorse, Sophie Novak and Alexandre Chevillot-Biraud (experimental officers at ITODYS lab) are acknowledged for their assistance with Raman, XPS, XRF, and TGA measurements, respectively.

Funding

We thank the China Scholarship Council for the provision of PhD scholarship to Mengqi Tang (No 202008310221). Wallonie Bruxelles International (WBI) is acknowledged for the provision of a grant "Bourse WBI Excellence World" (No Imputation 101386, Article Budgétaire 33.01.00.07). A.M.K. and M.M.C. would like to thank the French government for funding A.M.K.'s contribution through a fellowship granted by the French Embassy in Egypt (Institut Français d'Egypte).

Conflict of Interest

The authors declare no conflict of interest

References

Adewuyi, A. (2020). "Challenges and prospects of renewable energy in Nigeria: A case of bioethanol and biodiesel production." Energy Reports **6**: 77-88.

Akram, A., A. Ikhlaq, F. Javed, M. Kazmi and F. Qi (2021). "UV-irradiated fly ash-catalyzed Fenton-type process for the removal of paracetamol in wastewater: nickel, copper, and manganese as active sites." Desalination And Water Treatment **215**: 160-166.

Ali, I., S. Afshinb, Y. Poureshgh, A. Azari, Y. Rashtbari, A. Feizizadeh, A. Hamzezadeh and M. Fazlzadeh (2020). "Green preparation of activated carbon from pomegranate peel coated with zero-valent iron nanoparticles (nZVI) and isotherm and kinetic studies of amoxicillin removal in water." Environmental Science and Pollution Research **27**(29): 36732-36743.

Ali, I., I. Burakova, E. Galunin, A. Burakov, E. Mkrtchyan, A. Melezhik, D. Kurnosov, A. Tkachev and V. Grachev (2019). "High-Speed and High-Capacity Removal of Methyl Orange and Malachite Green in Water Using Newly Developed Mesoporous Carbon: Kinetic and Isotherm Studies." ACS Omega **4**(21): 19293-19306.

Ali, I., T. Kon'kova, V. Kasianov, A. Rysev, S. Panglisch, X. Y. Mbianda, M. A. Habila and N. AlMasoud (2021). "Preparation and characterization of nano-structured modified montmorillonite for dioxidine antibacterial drug removal in water." Journal of Molecular Liquids **331**: 115770.

Aoulad El Hadj Ali, Y., M. Ahrouch, A. Ait Lahcen, Y. Abdellaoui and M. Stitou (2022). "Recent Advances and Prospects of Biochar-based Adsorbents for Malachite Green Removal: A Comprehensive Review." Chemistry Africa.

Aruna, N. Bagotia, A. K. Sharma and S. Kumar (2021). "A review on modified sugarcane bagasse biosorbent for removal of dyes." Chemosphere **268**: 129309.

Ashraf, G. A., R. T. Rasool, M. Hassan, L. Zhang and H. Guo (2021). "Heterogeneous catalytic activation of BaCu-based M-hexaferrite nanoparticles for methylene blue degradation under photo-Fenton-like system." Molecular Catalysis **505**: 111501.

Bhaumik, M., A. Maity and H. G. Brink (2022). "Metallic nickel nanoparticles supported polyaniline nanotubes as heterogeneous Fenton-like catalyst for the degradation of brilliant green dye in aqueous solution." Journal of Colloid and Interface Science **611**: 408-420.

Biesinger, M. C. (2017). "Advanced analysis of copper X-ray photoelectron spectra." Surface and Interface Analysis **49**(13): 1325-1334.

Bokare, A. D. and W. Choi (2014). "Review of iron-free Fenton-like systems for activating H2O2 in advanced oxidation processes." Journal Of Hazardous Materials **275**: 121-135.

Boubkr, L., A. K. Bhakta, Y. Snoussi, C. Moreira Da Silva, L. Michely, M. Jouini, S. Ammar and M. M. Chehimi (2022) "Highly Active Ag-Cu Nanocrystal Catalyst-Coated Brewer’s Spent Grain Biochar for the Mineralization of Methyl Orange and Methylene Blue Dye Mixture." Catalysts **12** DOI: 10.3390/catal12111475.

Cao, B., J. Yuan, D. Jiang, S. Wang, B. Barati, Y. Hu, C. Yuan, X. Gong and Q. Wang (2021). "Seaweed-derived biochar with multiple active sites as a heterogeneous catalyst for converting macroalgae into acid-free biooil containing abundant ester and sugar substances." Fuel **285**: 119164.

Chen, X., J. Lin, Y. Su and S. Tang (2022) "One-Step Carbonization Synthesis of Magnetic Biochar with 3D Network Structure and Its Application in Organic Pollutant Control." International Journal of Molecular Sciences **23** DOI: 10.3390/ijms232012579.

Chen, X., W. Liu, J. Luo, H. Niu, R. Li and C. Liang (2022). "Structure Evolution of Ni–Cu Bimetallic Catalysts Derived from Layered Double Hydroxides for Selective Hydrogenation of Furfural to Tetrahydrofurfuryl Alcohol." Industrial & Engineering Chemistry Research **61**(35): 12953-12965.

da Silva Veiga, P. A., M. H. Cerqueira, M. G. Goncalves, T. T. da Silva Matos, G. Pantano, J. Schultz, J. B. de Andrade and A. S. Mangrich (2021). "Upgrading from batch to continuous flow process for the pyrolysis of sugarcane bagasse: Structural characterization of the biochars produced." Journal Of Environmental Management **285**.

da Silva Veiga, P. A., J. Schultz, T. T. da Silva Matos, M. R. Fornari, T. G. Costa, L. Meurer and A. S. Mangrich (2020). "Production of high-performance biochar using a simple and low-cost method: Optimization of pyrolysis parameters and evaluation for water treatment." Journal Of Analytical And Applied Pyrolysis **148**.

Deka, P., B. J. Borah, H. Saikia and P. Bharali (2019). "Cu-Based Nanoparticles as Emerging Environmental Catalysts." The Chemical Record **19**(2-3): 462-473.

Deraz, N. (2018). "The comparative jurisprudence of catalysts preparation methods: I. Precipitation and impregnation methods." J. Ind. Environ. Chem **2**(1): 19-21.

Dihingia, H. and D. Tiwari (2022). "Impact and implications of nanocatalyst in the Fenton-like processes for remediation of aquatic environment contaminated with micro-pollutants: A critical review." Journal of Water Process Engineering **45**: 102500.

Ding, H., G. Tong, J. Sun, J. Ouyang, F. Zhu, Z. Zhou, N. Zhou and M. e. Zhong (2023). "Regeneration of methylene blue-saturated biochar by synergistic effect of H2O2 desorption and peroxymonosulfate degradation." Chemosphere **316**: 137766.

Dong, Q., D. Yang, L. Luo, Q. He, F. Cai, S. Cheng and Y. Chen (2021). "Engineering porous biochar for capacitive fluorine removal." Separation And Purification Technology **257**.

Gong, Z., T. Ma and F. Liang (2021). "Syntheses of magnetic blackberry-like Ni@Cu@Pd nanoparticles for efficient catalytic reduction of organic pollutants." Journal of Alloys and Compounds **873**: 159802.

Gopinath, A., G. Divyapriya, V. Srivastava, A. R. Laiju, P. V. Nidheesh and M. S. Kumar (2021). "Conversion of sewage sludge into biochar: A potential resource in water and wastewater treatment." Environmental Research **194**: 110656.

Goswami, L., A. Kushwaha, S. R. Kafle and B.-S. Kim (2022). "Surface modification of biochar for dye removal from wastewater." Catalysts **12**(8): 817.

Hamouma, O., N. Kaur, D. Oukil, A. Mahajan and M. M. Chehimi (2019). "Paper strips coated with polypyrrole-wrapped carbon nanotube composites for chemi-resistive gas sensing." Synthetic Metals **258**: 116223.

Hu, L. Y., B. Yue, X. Y. Chen and H. Y. He (2014). "Direct hydroxylation of benzene to phenol on Cu-V bimetal modified HMS catalysts." Catalysis Communications **43**: 179-183.

Huang, Q., C. Chen, X. Zhao, X. Bu, X. Liao, H. Fan, W. Gao, H. Hu, Y. Zhang and Z. Huang (2021). "Malachite green degradation by persulfate activation with CuFe2O4@biochar composite: Efficiency, stability and mechanism." Journal of Environmental Chemical Engineering **9**(4): 105800.

Huang, Y., W. Su, R. Wang and T. Zhao (2019). "Removal of typical industrial gaseous pollutants: From carbon, zeolite, and metal-organic frameworks to molecularly imprinted adsorbents." Aerosol and Air Quality Research **19**(9): 2130-2150.

Jha, A., D.-W. Jeong, J.-O. Shim, W.-J. Jang, Y.-L. Lee, C. V. Rode and H.-S. Roh (2015). "Hydrogen production by the water-gas shift reaction using CuNi/Fe2O3 catalyst." Catalysis Science & Technology **5**(5): 2752-2760.

Jing, H., L. Ji, Z. Wang, J. Guo, S. Lu, J. Sun, L. Cai and Y. Wang (2021). "Synthesis of ZnO nanoparticles loaded on biochar derived from spartina alterniflora with superior photocatalytic degradation performance." Nanomaterials **11**(10): 2479.

Kant Bhatia, S., A. K. Palai, A. Kumar, R. Kant Bhatia, A. Kumar Patel, V. Kumar Thakur and Y.-H. Yang (2021). "Trends in renewable energy production employing biomass-based biochar." Bioresource Technology **340**: 125644.

Kasera, N., P. Kolar and S. G. Hall (2022). "Nitrogen-doped biochars as adsorbents for mitigation of heavy metals and organics from water: a review." Biochar **4**(1): 17.

Khalil, A. M., L. Michely, R. Pires, S. Bastide, K. Jlassi, S. Ammar, M. Jaziri and M. Chehimi (2021). "Copper/nickel-decorated olive pit biochar: One pot solid state synthesis for environmental remediation." Applied Sciences **11**(18).

Li, C.-Z. (2007). "Some recent advances in the understanding of the pyrolysis and gasification behaviour of Victorian brown coal." Fuel **86**(12): 1664-1683.

Li, D., L. Zhao, X. Cao, Z. Xiao, H. Nan and H. Qiu (2021). "Nickel-catalyzed formation of mesoporous carbon structure promoted capacitive performance of exhausted biochar." Chemical Engineering Journal **406**: 126856.

Li, Y., Y. Liu, Y. Liu, Y. Chen, L. Chen, H. Yan, Y. Chen, F. Xu, M. Li and L. Li (2022). "Modification of sludge biochar by MnO2 to degrade methylene blue: Synergistic catalysis and degradation mechanisms." Journal of Water Process Engineering **48**: 102864.

Liao, F., T. W. B. Lo and S. C. E. Tsang (2015). "Recent Developments in Palladium-Based Bimetallic Catalysts." ChemCatChem **7**(14): 1998-2014.

Liao, M. Z., C. Wang, E. Q. Bu, Y. Chen, Z. D. Cheng, X. L. Luo, R. Y. Shu and J. H. Wu (2018). Efficient hydrogen production from partial oxidation of propane over SiC doped Ni/Al2O3 catalyst. 10th International Conference on Applied Energy (ICAE), Hong Kong, HONG KONG.

Liu, H., Y. Liu, X. Li, X. Zheng, X. Feng and A. Yu (2022) "Adsorption and Fenton-like Degradation of Ciprofloxacin Using Corncob Biochar-Based Magnetic Iron–Copper Bimetallic Nanomaterial in Aqueous Solutions." Nanomaterials **12** DOI: 10.3390/nano12040579.

Liu, W.-J., H. Jiang and H.-Q. Yu (2015). "Development of Biochar-Based Functional Materials: Toward a Sustainable Platform Carbon Material." Chemical Reviews **115**(22): 12251-12285.

Liu, Y., Z. Jiang, J. Fu, W. Ao, A. Ali Siyal, C. Zhou, C. Liu, J. Dai, M. Yu, Y. Zhang, Y. Jin, Y. Yuan and C. Zhang (2022). "Iron-biochar production from oily sludge pyrolysis and its application for organic dyes removal." Chemosphere **301**: 134803.

Lopes, R. P. and D. Astruc (2021). "Biochar as a support for nanocatalysts and other reagents: Recent advances and applications." Coordination Chemistry Reviews **426**: 213585.

Low, Y. W. and K. F. Yee (2021). "A review on lignocellulosic biomass waste into biochar-derived catalyst: Current conversion techniques, sustainable applications and challenges." Biomass and Bioenergy **154**: 106245.

Nagula, S. and A. Ramanjaneyulu (2020). "Biochar-The New Black Gold." Biotica Research Today **2**(6): 425-427.

Nidheesh, P. V., R. Gandhimathi and S. T. Ramesh (2013). "Degradation of dyes from aqueous solution by Fenton processes: a review." Environmental Science and Pollution Research **20**(4): 2099-2132.

Omiri, J., Y. Snoussi, A. K. Bhakta, S. Truong, S. Ammar, A. M. Khalil, M. Jouini and M. M. Chehimi (2022). "Citric-Acid-Assisted Preparation of Biochar Loaded with Copper/Nickel Bimetallic Nanoparticles for Dye Degradation." Colloids and Interfaces **6**(2).

Pan, S., H. M. Zabed, Y. Wei and X. Qi (2022). "Technoeconomic and environmental perspectives of biofuel production from sugarcane bagasse: Current status, challenges and future outlook." Industrial Crops and Products **188**: 115684.

Pang, J., A. Wang, M. Zheng, Y. Zhang, Y. Huang, X. Chen and T. Zhang (2012). "Catalytic conversion of cellulose to hexitols with mesoporous carbon supported Ni-based bimetallic catalysts." Green Chemistry **14**(3): 614-617.

Quiton, K. G. N., M.-C. Lu and Y.-H. Huang (2021). "Synthesis and catalytic utilization of bimetallic systems for wastewater remediation: A review." Chemosphere **262**: 128371.
Radji, G., N. Bettahar, A. Bahmani, I. Boukhetache and S. Contreras (2022). "Heterogeneous Fenton-like degradation of organic pollutants in petroleum refinery wastewater by copper-type layered double hydroxides." Journal Of Water Process Engineering **50**.
Ramlingam, S., S. Subramanian and P. Ganesan (2022). Conversion of Agro Wastes to Solid and Gaseous Biofuels through Thermal Cracking Technique. Production Technologies for Gaseous and Solid Biofuels**:** 263-289.
Rangarajan, G. and R. Farnood (2022). "Role of persistent free radicals and lewis acid sites in visible-light-driven wet peroxide activation by solid acid biochar catalysts – A mechanistic study." Journal of Hazardous Materials **438**: 129514.
Rani, B., A. K. Nayak and N. K. Sahu (2022). "Degradation of mixed cationic dye pollutant by metal free melem derivatives and graphitic carbon nitride." Chemosphere **298**: 134249.
Saravanan, A., P. S. Kumar, N. S. Mat Aron, S. Jeevanantham, S. Karishma, P. R. Yaashikaa, K. W. Chew and P. L. Show (2022). "A review on bioconversion processes for hydrogen production from agro-industrial residues." International Journal of Hydrogen Energy **47**(88): 37302-37320.
Sharma, G., S. Bhogal, V. K. Gupta, S. Agarwal, A. Kumar, D. Pathania, G. T. Mola and F. J. Stadler (2019). "Algal biochar reinforced trimetallic nanocomposite as adsorptional/photocatalyst for remediation of malachite green from aqueous medium." Journal of Molecular Liquids **275**: 499-509.
Shi, Q., S. Deng, Y. Zheng, Y. Du, L. Li, S. Yang, G. Zhang, L. Du, G. Wang and M. Cheng (2022). "The application of transition metal-modified biochar in sulfate radical based advanced oxidation processes." Environmental Research **212**: 113340.
Snoussi, Y., S. Bastide, M. Abderrabba and M. M. Chehimi (2018). "Sonochemical synthesis of Fe3O4@NH2-mesoporous silica@Polypyrrole/Pd: A core/double shell nanocomposite for catalytic applications." Ultrasonics Sonochemistry **41**: 551-561.
Snoussi, Y., I. Sifaoui, M. El Garah, A. M. Khalil, J. E. Piñero, M. Jouini, S. Ammar, J. Lorenzo-Morales and M. M. Chehimi (2023). "Green, zero-waste pathway to fabricate supported nanocatalysts and anti-kinetoplastid agents from sugarcane bagasse." Waste Management **155**: 179-191.
Soon, A. N. and B. H. Hameed (2011). "Heterogeneous catalytic treatment of synthetic dyes in aqueous media using Fenton and photo-assisted Fenton process." Desalination **269**(1): 1-16.
Sun, H., D. Feng, Y. Zhang, S. Sun, Y. Zhao and F. Zhang (2022). "Roles of AAEMs in catalytic reforming of biomass pyrolysis tar and coke accumulation characteristics over biochar surface for H2 production." International Journal of Hydrogen Energy **47**(68): 29207-29218.
Sutar, S., P. Patil and J. Jadhav (2022). "Recent advances in biochar technology for textile dyes wastewater remediation: A review." Environmental Research: 112841.
Tang, C., M. Cheng, C. Lai, L. Li, X. Yang, L. Du, G. Zhang, G. Wang and L. Yang (2023). "Recent progress in the applications of non-metal modified graphitic carbon nitride in photocatalysis." Coordination Chemistry Reviews **474**: 214846.
Tang, M., Y. Snoussi, A. Bhakta, M. El Garah, A. Khalil, S. Ammar and M. Chehimi (2022). "Unusual, hierarchically structured composite of sugarcane pulp bagasse biochar loaded with Cu/Ni bimetallic nanoparticles."
Tripathi, M., J. N. Sahu and P. Ganesan (2016). "Effect of process parameters on production of biochar from biomass waste through pyrolysis: A review." Renewable and Sustainable Energy Reviews **55**: 467-481.
Verma, P., Y. Kuwahara, K. Mori, R. Raja and H. Yamashita (2020). "Functionalized mesoporous SBA-15 silica: recent trends and catalytic applications." Nanoscale **12**(21): 11333-11363.
Wang, C., R. Sun and R. Huang (2021). "Highly dispersed iron-doped biochar derived from sawdust for Fenton-like degradation of toxic dyes." Journal of Cleaner Production **297**: 126681.

Wang, L., Y. Liu, Y. Lin, Y. Yu, X. Zhang, R. Zhang and Y. Zhai (2021). "One-step synthesis of novel Ni-doped Cu2(OH)3F Fenton-like catalyst driven by visible light: Single activity and synergistic effect enhanced by bimetallic cooperation." Journal of Alloys and Compounds **887**: 161424.

Wang, N., Q. Sun, T. Zhang, A. Mayoral, L. Li, X. Zhou, J. Xu, P. Zhang and J. Yu (2021). "Impregnating subnanometer metallic nanocatalysts into self-pillared zeolite nanosheets." Journal of the American Chemical Society **143**(18): 6905-6914.

Wang, Q., Y. Ma and S. T. Xing (2018). "Comparative study of Cu-based bimetallic oxides for Fenton-like degradation of organic pollutants." Chemosphere **203**: 450-456.

Wolfbeisser, A., G. Kovács, S. M. Kozlov, K. Föttinger, J. Bernardi, B. Klötzer, K. M. Neyman and G. Rupprechter (2017). "Surface composition changes of CuNi-ZrO2 during methane decomposition: An operando NAP-XPS and density functional study." Catalysis Today **283**: 134-143.

Wu, Y., S. Zeng, F. Wang, M. Megharaj, R. Naidu and Z. Chen (2015). "Heterogeneous Fenton-like oxidation of malachite green by iron-based nanoparticles synthesized by tea extract as a catalyst." Separation and Purification Technology **154**: 161-167.

Xavier, S., R. Gandhimathi, P. V. Nidheesh and S. T. Ramesh (2015). "Comparison of homogeneous and heterogeneous Fenton processes for the removal of reactive dye Magenta MB from aqueous solution." Desalination And Water Treatment **53**(1): 109-118.

Xia, J., Y. Shen, H. Zhang, X. Hu, M. M. Mian and W.-H. Zhang (2022). "Synthesis of magnetic nZVI@biochar catalyst from acid precipitated black liquor and Fenton sludge and its application for Fenton-like removal of rhodamine B dye." Industrial Crops and Products **187**: 115449.

Xia, Z., M. Li, H. Hao, Q. Zhang, M. Zhong, Y. Qiu, X. Wei and Z. Fan (2023). "The role of nonradicals in simultaneous degradation and detoxification of Malachite Green via biochar decorated with δ-MnO2." Environmental Technology & Innovation **29**: 102992.

Xiao, W., M. Cheng, Y. Liu, J. Wang, G. Zhang, Z. Wei, L. Li, L. Du, G. Wang and H. Liu (2023). "Functional Metal/Carbon Composites Derived from Metal–Organic Frameworks: Insight into Structures, Properties, Performances, and Mechanisms." ACS Catalysis **13**: 1759-1790.

Yameen, M. Z., H. AlMohamadi, S. R. Naqvi, T. Noor, W.-H. Chen and N. A. S. Amin (2023). "Advances in production & activation of marine macroalgae-derived biochar catalyst for sustainable biodiesel production." Fuel **337**: 127215.

Zarei, M., I. Mohammadzadeh, K. Saidi and H. Sheibani (2022). "Fabrication of biochar@Cu-Ni nanocatalyst for reduction of aryl aldehyde and nitroarene compounds." Biomass Conversion and Biorefinery.

Zarei, M., K. Saidi and H. Sheibani (2022). "Preparation and investigation of catalytic activities of Cu-Ni nanoparticles supported on the biochar derived from pomegranate shells in the A3-coupling reactions." Biomass Conversion and Biorefinery.

zhang, Y., X. Li, J. Chen, Y. Wang, Z. Cheng, X. Chen, X. Gao and M. Guo (2023). "Porous spherical Cu2O supported by wood-based biochar skeleton for the adsorption-photocatalytic degradation of methyl orange." Applied Surface Science **611**: 155744.

Zhu, C., H. Wang, H. Li, B. Cai, W. Lv, C. Cai, C. Wang, L. Yan, Q. Liu and L. Ma (2019). "Selective Hydrodeoxygenation of 5-Hydroxymethylfurfural to 2,5-Dimethylfuran over Alloyed Cu−Ni Encapsulated in Biochar Catalysts." ACS Sustainable Chemistry & Engineering **7**(24): 19556-19569.

Zhu, H. and H. Zou (2022). "Ultra-efficient catalytic degradation of malachite green dye wastewater by KMnO4-modified biochar (Mn/SRBC)." RSC Advances **12**(41): 27002-27011.

1